Open access • Journal Article • DOI:10.1007/S00107-018-1376-Y

Use of particle tracking velocimetry in timber material and connection testing

Lisa-Mareike Ottenhaus, Minghao Li, Roger Nokes, Peter Cammock ...+1 more authors

Institutions: University of Canterbury

Published on: 01 Mar 2019 - European Journal of Wood and Wood Products (Springer Berlin Heidelberg)

Topics: Cross laminated timber, Embedment, Dowel, Laminated veneer lumber and Particle tracking velocimetry

European Journal of Wood and Wood Products

Use of Particle Tracking Velocimetry in Timber Material and Connection Testing

--Manuscript Draft--

Manuscript Number:	HARW-D-18-00084R2
Full Title:	Use of Particle Tracking Velocimetry in Timber Material and Connection Testing
Article Type:	Original Article
Corresponding Author:	Lisa-Mareike Ottenhaus, MSc University of Canterbury Christchurch, New Zealand NEW ZEALAND
Corresponding Author Secondary Information:	
Corresponding Author's Institution:	University of Canterbury
Corresponding Author's Secondary Institution:	
First Author:	Lisa-Mareike Ottenhaus, MSc
First Author Secondary Information:	
Order of Authors:	Lisa-Mareike Ottenhaus, MSc
	Minghao Li
	Roger Nokes
	Peter Cammock
	Braeden McInnes
Order of Authors Secondary Information:	
Author Comments:	WCTE2018 paper is now published
Response to Reviewers:	Thank you for this comment. Several highlighted sentences have been added to explain the choice of PTV over DIC and MTM. Furthermore, a reference has been added that demonstrates the advantages of MTM (which is similar to PTV). The authors are not aware of a publication that compares PTV to these methods as PTV is not (yet) commonly used in structural engineering.

Use of Particle Tracking Velocimetry in Timber Material and Connection Testing

Lisa-Mareike Ottenhaus[1], Minghao Li[2], Roger Nokes[3], Peter Cammock[4], Braeden McInnes[5]

[1-5] Department of Civil and Natural Resources Engineering, University of Canterbury, New Zealand
[1] lisa-mareike.ottenhaus@pg.canterbury.ac.nz; 0000-0001-7129-8017: corresponding author
[2] minghao.li@canterbury.ac.nz;
[3] roger.nokes@canterbury.ac.nz

ABSTRACT:

Particle Tracking Velocimetry (PTV) is a quantitative field measuring technique originally developed to track and measure the velocity of individual particles in fluid flows. In this study, PTV was applied for the first time in three different experimental studies in the field of structural timber engineering: 1) dowel embedment testing in Cross Laminated Timber (CLT), 2) large-scale dowelled CLT connection testing, 3) material testing of small clear wood and Laminated Veneer Lumber (LVL). The suitability of PTV was first assessed by comparing the PTV displacements to those obtained by potentiometers. Furthermore, the behaviour of the timber substrate was analysed with PTV in both embedment and large-scale connection tests. It was found that PTV was able to not only accurately measure dowel displacements, but also capture crack growth in the timber and compute the resulting displacement and strain fields in the dowel embedment area. Lastly, PTV was applied in small clear specimen testing to capture brittle fracture in shear, tension perpendicular to the grain, and in cleavage. This study demonstrated that PTV is able to provide reliable contact-free high-resolution measurements of displacement and strain fields on exposed timber surfaces and capture failure mechanisms such as brittle fractures and crack growth.

KEYWORDS: Particle Tracking Velocimetry, Timber Testing, Displacement, Strain, Connection, Small Clear Wood

ACKNOWLEDGEMENTS

The research was jointly funded by the Natural Hazards Research Platform and EQC Post-graduate Research Grant in New Zealand. XLam NZ Ltd. is gratefully acknowledged for supplying the CLT.

1 INTRODUCTION

Contact-free strain and displacement field measurements have gained popularity in the last 30 years or so as they provide hundreds of measuring points per experiment as opposed to conventional position and strain sensors such as potentiometers, Linear Variable Differential Transformers (LVDTs), and strain gauges that only measure one point per device. Furthermore, potentiometers, LVDTs, and strain gauges must be physically attached to the test specimen and therefore always represent a potential source of interference with the experiment (Mokhtari et al. 2017).

Digital Image Correlation (DIC) is a popular contact-free deformation/strain measuring technique in many fields of engineering that dates back to the end of the last century when images were captured on film and then digitalized (Sutton et al. 1983, Choi et al. 1991, Samarasinghe et al. 1997). Simply speaking, DIC compares digital images of the test specimen's surface at different stages of deformation. The light intensity pattern of a pixel subset of the first image is stored and recognized in the subsequent images. By cross-correlating several subset pairs, a strain or deformation field can be calculated (Pan et al. 2009, McCormick and Lord 2010). Nowadays, DIC is widely accepted and commonly used in research and practice. In the field of structural timber engineering, DIC has been successfully combined with the Finite Element Method (FEM) and has been used in practice to monitor building deformations (Murata et al. 2005, Dubois et al. 2012, van Beerschoten et al. 2014, Henke et al. 2015).

A variation of the DIC technique is the Mark Tracking Method (MTM) where high contrast marks or paint dots are applied to the specimen surface (Chean et al. 2011, Pop and Dubois 2016). Applying distinct marks has the advantage that they can be easier to track which can reduce noise in practical applications and facilitate the capturing of discontinuous processes such as crack growth and fracture. Furthermore, MTM allows to generate strain and displacement fields and estimate fracture parameters without needing to establish mechanical behaviour laws (Bretagne et al. 2005, Pop and Dubois 2016).

Particle Image Velocimetry (PIV) and Particle Tracking Velocimetry (PTV) are both quantitative field measuring techniques originating in fluid mechanics based on the principle of capturing video images of a particle seeded fluid flow, and from that video record extracting quantitative information about the flow field (Adrian 2005, Chenouard et al. 2014, Qiao et al. 2016, Crowe et al. 2016, Zhou et al 2017, Nokes 2017).

PIV is very similar to DIC in that it uses the cross-correlation of the intensity fields in two consecutive images to obtain fluid velocities from peaks in the cross-correlation field. In structural applications PIV has the additional advantage that it contains a time component which allows it not only to map strains and deformations but also to measure accelerations e.g. in shake-table tests. In structural timber engineering, PIV has recently been successfully implemented to visualize strain fields in a deforming Cross Laminated Timber (CLT) slab (Papastavrou et al. 2016).

PTV on the other hand is similar to MTM as it identifies individual particles and tracks them across images in order to establish particle-centred velocity estimates. As PTV is very commonly used in fluid mechanics, a range of

sophisticated image processing tools is available. Furthermore, the time component of the particle records presents an opportunity to measure accelerations (e.g. during dynamic testing) in future applications. This paper presents how PTV can be extended to structural engineering research, thereby replacing conventional position sensors and strain sensors while improving the data resolution.

In this research, the image processing and PTV system *Streams* was used for the first time in the context of structural timber testing (Ottenhaus et al. 2018). The versatility of PTV was demonstrated on three different experimental setups: dowel embedment tests, large-scale dowelled connection tests, and small clear wood and LVL testing.

2 METHODOLOGY

PTV in structural testing consists of the following two main steps:

1) Preparation and experimental testing

- Experimental setup
- Particle application
- Camera setup and lighting
- Image capture during experimental testing

2) Post processing and PTV analysis

- Image processing and particle identification
- Particle tracking
- Displacement field generation
- Strain field generation

Step 1 will be briefly outlined in the following but has been explained in detail in Ottenhaus et al. (2018). This paper focuses on step 2 and quantitative evaluations of the displacement and strain fields.

2.1 PREPARATION AND EXPERIMENTAL TESTING

Different experiments require different displacement and strain measurements. In the following, three different test setups are described and it is highlighted how PTV was applied differently in each of them. For the embedment and large-scale connection tests, Digital Single-Lens Reflex (DSLR) cameras were mounted at the centroid of the test area on each side of the test specimen with sufficient distance from the specimen surface to avoid distortions. For small clear testing, only one side of the specimen was captured as cracks typically develop symmetrically through the entire thickness of the specimens.

2.1.1 Test setup: Embedment tests

A total of 101 half-hole embedment tests were carried out according to ASTM D5764 – 97a (2013) on three-layer CLT specimens made of New Zealand *radiata pine*. The dowel sizes were 12, 16, and 20 mm and the load was applied evenly across the dowels with a load displacement rate of 2 mm/min. The displacements were measured with a LVDT

and by means of PTV with a scale of 0.035 mm/px. To achieve this, a regular pattern of 1.2 mm diameter matt white particles spaced at 2.6 mm in the loading direction and 4.0 mm in the perpendicular direction was applied to the timber substrate. For this purpose, a piece of perforated foil was applied to the timber surface and matt white paint was applied with a fine brush. One DSLR camera was mounted on each side of the specimen at approximately 1 m distance from the timber surface and four Compact Fluorescent Lamps (CFLs) were installed at the specimen corners to achieve an even light intensity distribution. The data and image acquisition were synchronized and triggered every 2 seconds. Furthermore, a mesh of reference particles was captured in each image to later subtract background vibrations as shown in Figure 1.

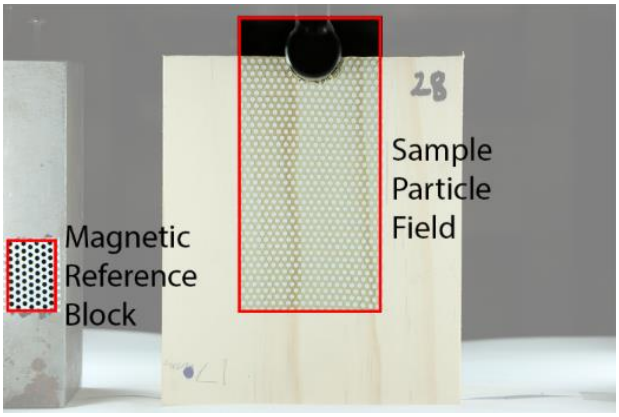

Fig. 1 Test setup of embedment tests.

2.1.2 Test setup: Large-scale dowelled connection tests

A total of 12 *radiata pine* CLT panels with three different layouts of dowelled connections were subjected to monotonic and cyclic loading (Ottenhaus et al. 2017, 2018). While the experiments were displacement controlled, the nature of the hydraulic jacks did not allow for a constant displacement rate to be applied. The displacements were recorded with three string potentiometers on each side of the connection, and captured with PTV every 2 seconds as shown in Figure 2. For this purpose, a regular mesh of 1.2 mm diameter particles spaced at 4.0 mm in the loading direction and 2.6 mm in the perpendicular direction was applied to the timber substrate. One DSLR camera was mounted at each side of the panel, located 1.5 m from the panel surface. The PTV scale ranged from 0.19 to 0.26 mm/px depending on the size of the captured connection area. The fasteners and potentiometer attachment points (s_k) were coated in matt black paint and green labels were attached to the fasteners for the purpose of numbering and particle tracking (Figure 2a). Furthermore, a set of reference particles was applied to each potentiometer mount to later subtract background vibrations. Fluorescent light racks were mounted beneath the cameras to eliminate shadows and provide consistent lighting conditions during testing (Figures 2b and 2c).

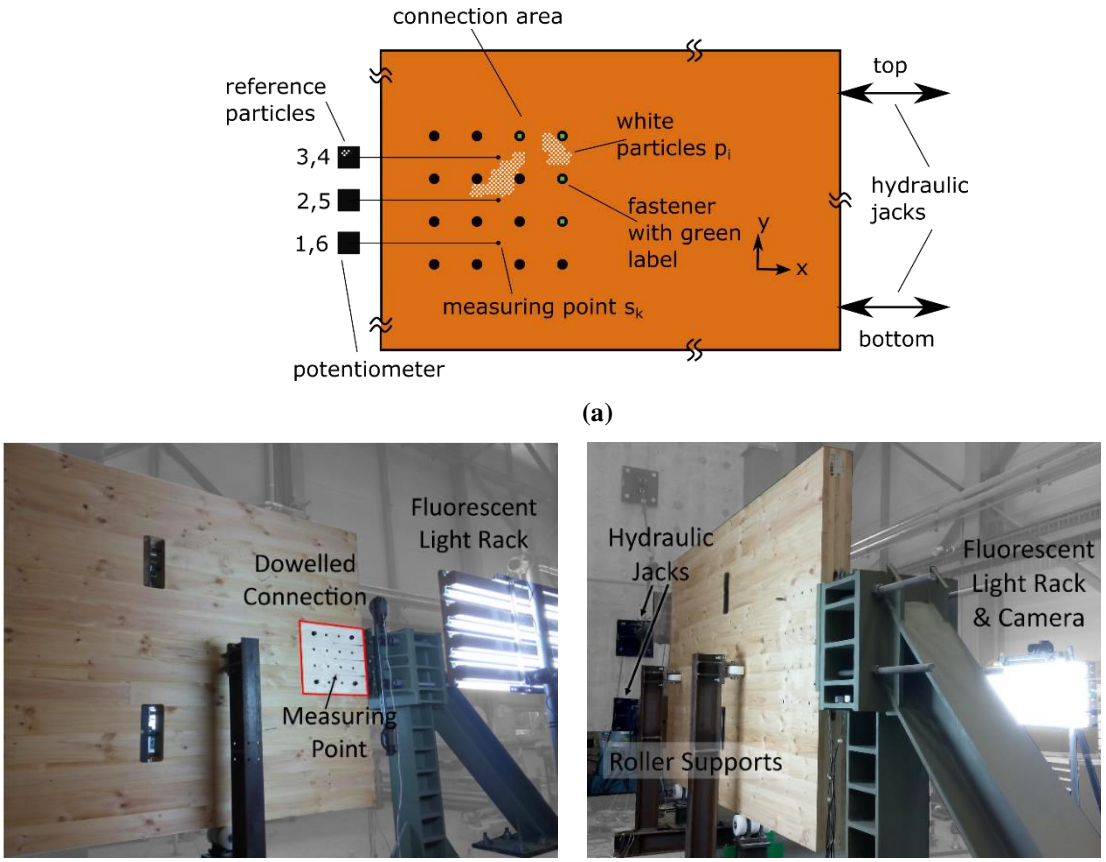

Fig. 2 Test setup of large-scale dowelled connection test: a) view from back, b) view from front, c) view along panel prior to particles application.

2.1.3 Test setup: Small clear specimens

A total of 79 small clear specimens of *radiata pine* wood and LVL were subjected to shear, tensile perpendicular to the grain, and cleavage tests according to ASTM D143-09 (2009) with the test setups shown in Figures 3a, 3b, and 3c, respectively. The displacement rate was 2 mm/min for both cleavage and tensile perpendicular to the grain tests, and 0.5 mm/min for shear tests. The specimens were coated in a thin layer of matt white paint and a random mesh of densely spaced black particles was manually applied. The particle size varied from 0.5 to 1.2 mm in diameter and particles spacing ranged from 1 to 4 mm, with particles being more densely spaced in the expected crack location as can be seen in Figures 3b and 3c. This was necessary as the mesh obtained with the perforated foil in embedment and large-scale testing was too coarse to adequately capture crack growth. Images were captured twice per second with one DSLR camera as the specimens were thin enough for cracks to grow through the entire specimen thickness. The PTV scale was 0.0266 mm/px for shear testing, 0.027 mm/px for cleavage testing, and 0.03 mm/px for tensile perpendicular to the grain testing. A fluorescent light rack alongside several spot lights was used to achieve even illumination of the specimens. Furthermore, reference particles were captured in each image to capture background vibrations.

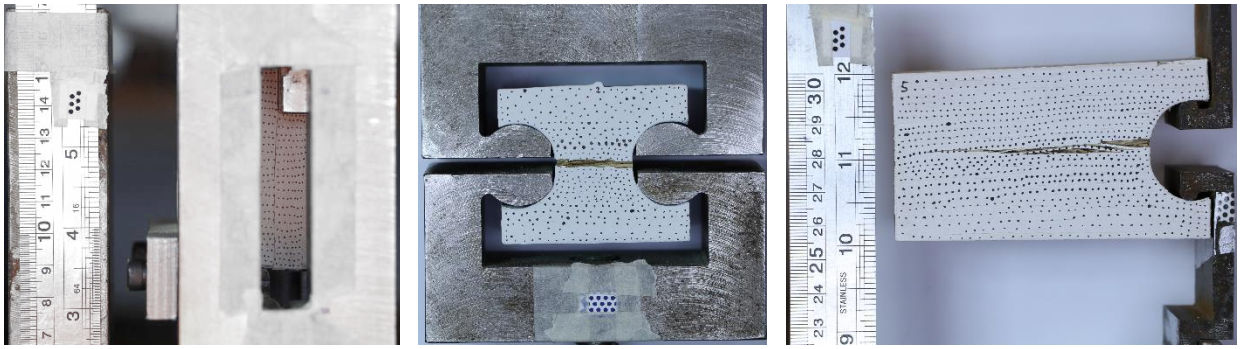

(a) **(b)** **(c)**

Fig. 3 Test setup of small clear tests: a) shear, b) tension perpendicular to the grain, c) cleavage.

2.2 IMAGE PROCESSING AND PARTICLE TRACKING VELOCIMETRY

Particle identification algorithms generally require the ability to identify pixels that comprise the particles. Often this is achieved through differences in colour or intensity and this requirement needs to be considered when designing the experimental setup. In the following, image post-processing techniques and PTV processes that produced good results in this particular study are described. The described methods therefore represent a case study of PTV rather than an extensive introduction to PTV in structural timber applications.

2.2.1 Particle identification

In order to identify a particle, the captured images are searched for contiguous subsets of pixels all of whose intensities I_i exceed a user specified intensity threshold I_s. Within an area of interest containing n pixels, the particle's location (x_p, y_p) is then defined as the weighted average of those pixels' coordinates (x_i, y_i) as shown in Equation 1:

$$\begin{cases} x_p = \dfrac{\sum_i x_i I_i H(I_i - I_s)}{\sum_i I_i H(I_i - I_s)} \\ y_p = \dfrac{\sum_i y_i I_i H(I_i - I_s)}{\sum_i I_i H(I_i - I_s)} \end{cases} \quad i = 1 \dots n \qquad (1)$$

$$H(x) = \begin{cases} 0; x < 0 \\ 1; x \geq 0 \end{cases} \qquad (2)$$

where (x_i, y_j) are a pixel's coordinates, I_i is the pixel's intensity level, I_s is the intensity threshold and H is the Heaviside function as defined in Equation 2. This analysis is then repeated for each time step t. Additionally, particle size and aspect ratio can be used to help distinguish between those pixels lying inside or outside of a particle. The white particles in Figure 4 for instance were round particles with a 1.2 mm diameter. The images were thus searched for high intensity pixel subsets with a diameter between 0.9 and 1.5 mm and a maximum aspect ratio of 1.5.

As PTV relies on the identification of particles through intensity differences, it can be helpful to pre-process the images in order to generate stronger intensity contrasts. Examples of this pre-processing are illustrated on the experimental

tests that were part of this study. However, it should be noted that the image processing required will be dependent on the particular experimental configuration and therefore the examples below are for illustrative purposes only. *Streams* provides an extensive set of image processing algorithms and these are described in the software manuals (Nokes 2017).

In order to identify white particles in the embedment tests, all pixels below a certain blue intensity threshold were removed to amplify the contrast between the particles and the timber substrate as shown in Figure 4. This method also worked well for the white paint particles in large-scale embedment testing.

Several test setups resulted in dark particles on a light substrate, such as the potentiometer attachment points in large-scale connection testing or the black particles in small clear testing. In order to identity the particles with the algorithm given in Equation 1, it was necessary to invert the images as shown in Figure 5a.

For the identification of the green labels on the dowels in large-scale connection testing, it was chosen to subtract red and then amplify the green channel as can be seen in Figure 5b.

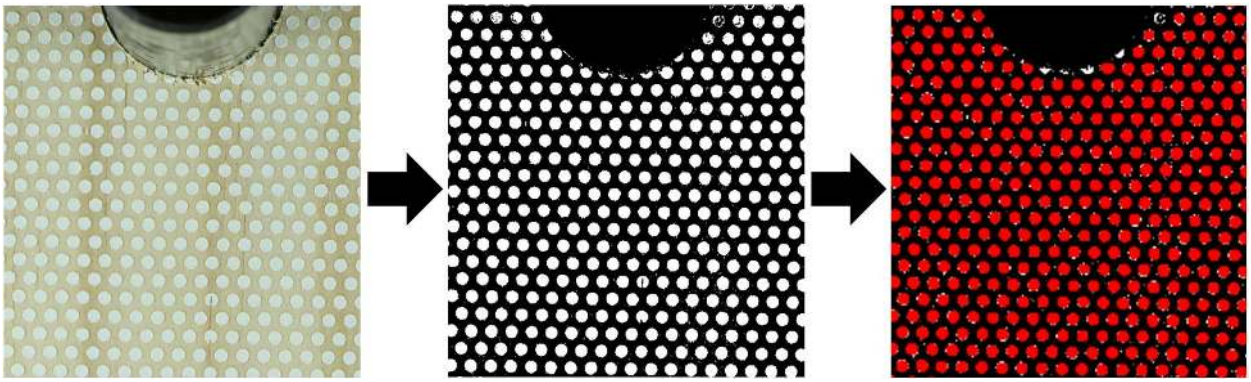

Fig. 4 Particle identification in embedment tests: Raw image, removal of low blue intensities, particle identification.

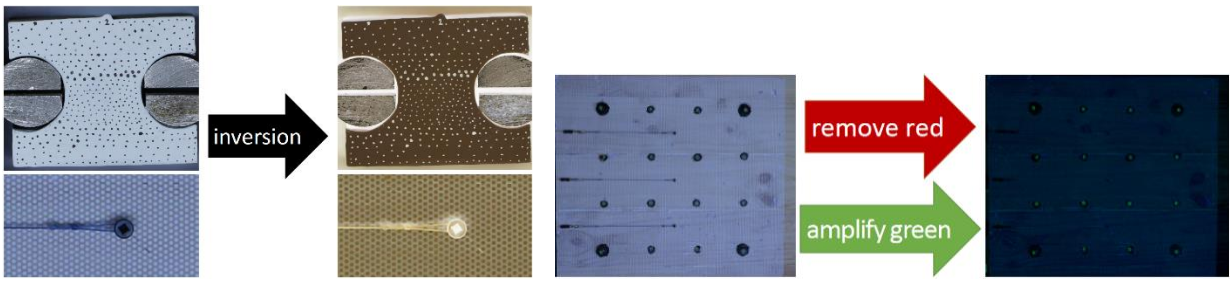

(a) **(b)**

Fig. 5 Image processing to achieve strong intensity contrasts.

2.2.2 Particle tracking

PTV is based on tracking m individual particles, p, across subsequent images or time steps, t, and storing their respective location (x_p, y_p) for each time step. After each time increment, Δt, a particle can be located in m possible new locations with m displacement vectors, $\mathbf{d_j}$, pointing to those locations as shown in Figure 6 and Equation 3. Each

particle thus has *m* possible matches. In order to assign the correct displacement vector, $\mathbf{d_p}$, an optimisation algorithm can be used to determine the desirability of a possible match and then allocate these matches between two times steps. A simple optimisation algorithm is distance based particle matching, where the correct displacement vector, $\mathbf{d_p}$, is assigned by finding the closest particle as shown in Equation 4. Distance based particle matching produced good results with acceptable computational cost for both embedment and connection tests as these experienced displacements that were generally smaller than the distance between particles.

The small clear specimens on the other hand experienced sudden failure with large displacements. Furthermore, both the specimens and failure planes were small. As a consequence a much denser mesh of fine particles had to be applied to capture crack growth and failure. In order to find the correct particle matches, correlation based particle matching was employed. Particle patterns in time step t were correlated to a pattern in time step $t + \Delta t$ in a manner similar to DIC. This method has the advantage that it generally finds the correct matches but requires more randomly distributed particles to be able to recognize patterns.

The respective matching process was then repeated for each time step to create a particle path. Finally, spurious particle paths were removed based on their path length or by comparing each particle's path to the paths of its surrounding particles.

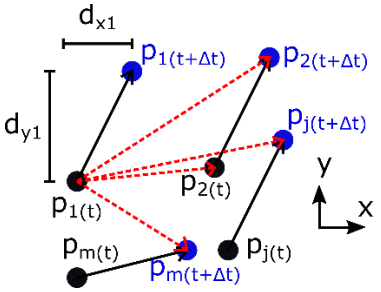

Fig. 6 Particle matching.

$$\boldsymbol{d_j} = \begin{pmatrix} d_{xj} \\ d_{yj} \end{pmatrix}$$

$$\begin{cases} d_{xj}(t) = x_j(t + \Delta t) - x_j(t) \\ d_{yj}(t) = y_j(t + \Delta t) - y_j(t) \end{cases} \quad j = 1 \dots m \tag{3}$$

$$\boldsymbol{d_p} = \begin{pmatrix} d_{xp} \\ d_{yp} \end{pmatrix} \xrightarrow{min\|\boldsymbol{d_j}\|} \boldsymbol{d_j}; j = 1 \dots m$$

$$\begin{cases} x_p(t + \Delta t) = x_p(t) + d_{xp} \\ y_p(t + \Delta t) = y_p(t) + d_{yp} \end{cases} \quad p = 1 \dots m \tag{4}$$

2.2.3 Removal of background vibrations

As mentioned previously, reference particles were captured in each image of each test setup. The reference particles were applied to a magnetic block for embedment testing. For large-scale connection testing, reference particles were applied to the potentiometer mounts, and for small clear testing they were located on the loading jaws. This was done in order to eliminate the influence of camera movement and ambient background vibrations on the PTV data sets. A path field was computed for each set of reference particles and their average displacement vector, $\mathbf{d_{ref}}$, was subtracted from the respective particle displacement vectors, $\mathbf{d_p}$, to compute the relative particle displacement, $\mathbf{d_p}^*$, as shown in Equation 5.

$$\boldsymbol{d_p^* = d_p - d_{ref}} \tag{5}$$

2.2.4 Displacement fields

Material based displacement fields were calculated from particle paths for each time step *t* using an interpolation method based on a method of Cline and Renka (1984) that uses a Delaunay triangulation (also known as Thiessen triangulation) as the basis for the interpolation between particles. Similar to the FEM, this method aims to maximize the minimum internal angle of the triangles, thereby interpolating between three particles that lie spatially close together. The lower bound of the triangle size was determined by the average particle distance in the x- and y-direction. Additionally, an upper bound for the triangle size was defined in the context of embedment and small clear testing to avoid interpolation over the gaps in the specimens.

2.2.5 Strain fields

A strain field was obtained for each time step *t* by computing the partial derivatives of the displacement vectors ***d****(t)* with respect to x and y for each particle as given in Equation 6. Cumulative strain fields can be computed for the elastic and plastic range of monotonic experiments, or for a time interval which is useful for cyclic testing. After onset of surface cracking, an equivalent cumulative surface strain can be obtained with Equation 6 which can serve for qualitative comparisons between experimental test results and FEM results.

$$\varepsilon_{xx} = \frac{d_x(t)}{dx};\ \varepsilon_{yy} = \frac{d_y(t)}{dy};\ \gamma_{xy} = \frac{d_x(t)}{dy} + \frac{d_y(t)}{dx} \tag{6}$$

2.2.6 Resolution and accuracy

The spatial resolution of PTV measurements depends on the particle density, i.e. the distance in the x- and y-direction between particles. A fine mesh of densely spaced particles can thus result in higher resolution, however, each particle should still consist of a clearly identifiable cluster of pixels, which is limited by the PTV scale (mm/px). The accuracy

of displacement calculations achieved with the processing software was +/- 0.25 px. As this absolute error stays constant the relative error decreases with increasing displacements.

3 RESULTS AND DISCUSSION

The PTV results obtained from the aforementioned embedment tests, large-scale connection tests, and small clear wood and LVL tests are discussed and contrasted with the results obtained with conventional measuring techniques. Furthermore, the advantages of PTV in terms of data quantity and quality are highlighted for each application.

3.1 EMBEDMENT TESTS

The displacement of the loading head was recorded for each time step *t* using an LVDT as specified in ASTM D5764 – 97a (2013). Additionally, the displacement and strain fields of the wood underneath the dowel were computed for each time step by means of PTV. Figure 7a displays the load versus time diagram of an embedment test. As the displacement rate was constant, the diagram is similar to the load-displacement diagram. Figure 7b shows the displacement vectors at $t = 604$s which is marked with a cross in Figure 7a. At this point, the dowel was fully embedded and a crack had started to form underneath the dowel. Figure 7c shows the cumulative y displacements 5 mm below the initial dowel position at different time steps *t*. Figure 7d displays the cumulative shear strain field at $t = 604$s.
In contrast to conventional LVDTs that only record the displacement of one specific location over time, PTV is able to capture entire displacement fields and compute the corresponding strain fields, thereby significantly increasing the number of measurement points. Furthermore, in this specific embedment test setup LVDTs are only able to provide indirect displacement measurements of either the loading head or the dowel ends. While it is possible to mount additional LVDTs and strain gauges to the specimen, these can interfere with the experiment itself, especially when the specimen dimensions are relatively small.

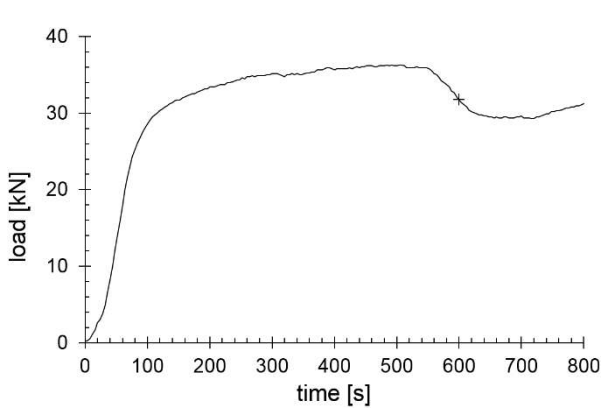

(a)

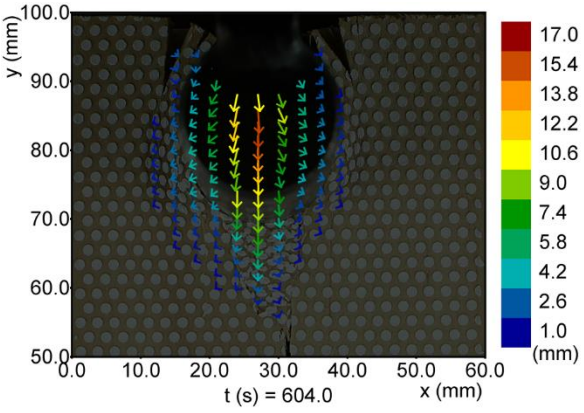

(b)

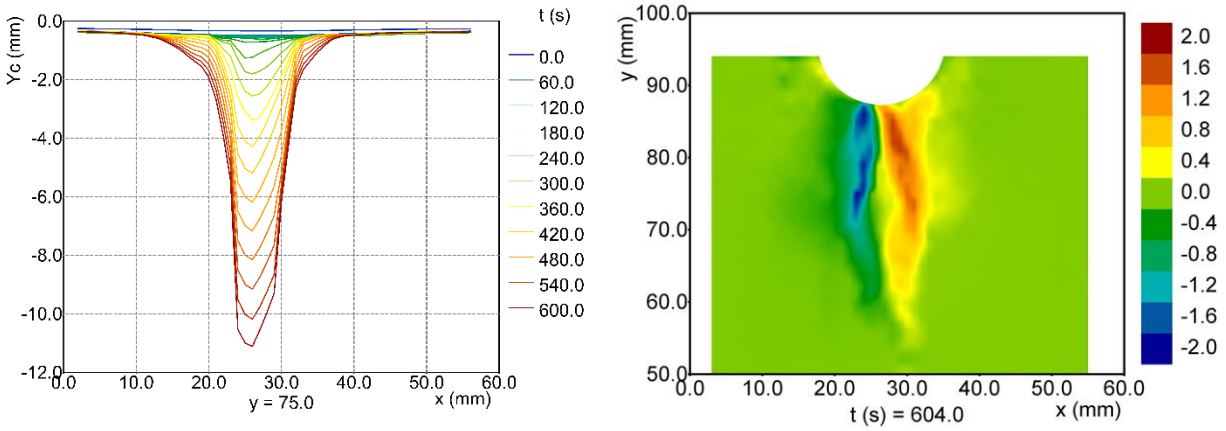

(c) **(d)**

Fig. 7 Dowel displacement and strain fields: a) load vs time, b) displacement vectors, c) cumulative vertical displacement underneath dowel vs time, d) cumulative shear strain field.

Figure 8a displays the displacement vectors of an embedment test that experienced significant cracking. As LVDTs only register unidirectional displacements, these displacements perpendicular to the loading direction were not recorded. PTV on the other hand was able to capture displacements in all directions, making it a suitable measuring technique for experiments where the response of the specimen is not predetermined. The cumulative y displacements for different time steps *t* are displayed in Figure 8b.

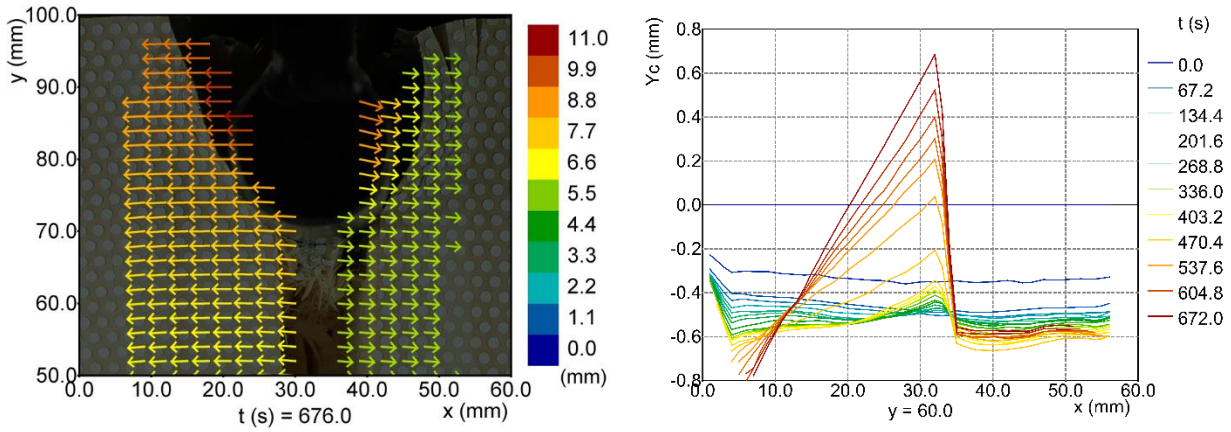

(a) **(b)**

Fig. 8 Dowel displacement: a) displacement vectors, b) cumulative vertical displacement underneath dowel vs time.

3.2 LARGE-SCALE CONNECTION TESTS

The versatility of PTV within one experiment is demonstrated by the results of a large-scale connection test. The displacements of potentiometer measuring points s_k were computed with PTV and compared to the potentiometer readings. Additionally, dowel displacements and timber crack growth between dowels were captured with PTV. All of these analyses were conducted on the same set of images as shown in Figure 9.

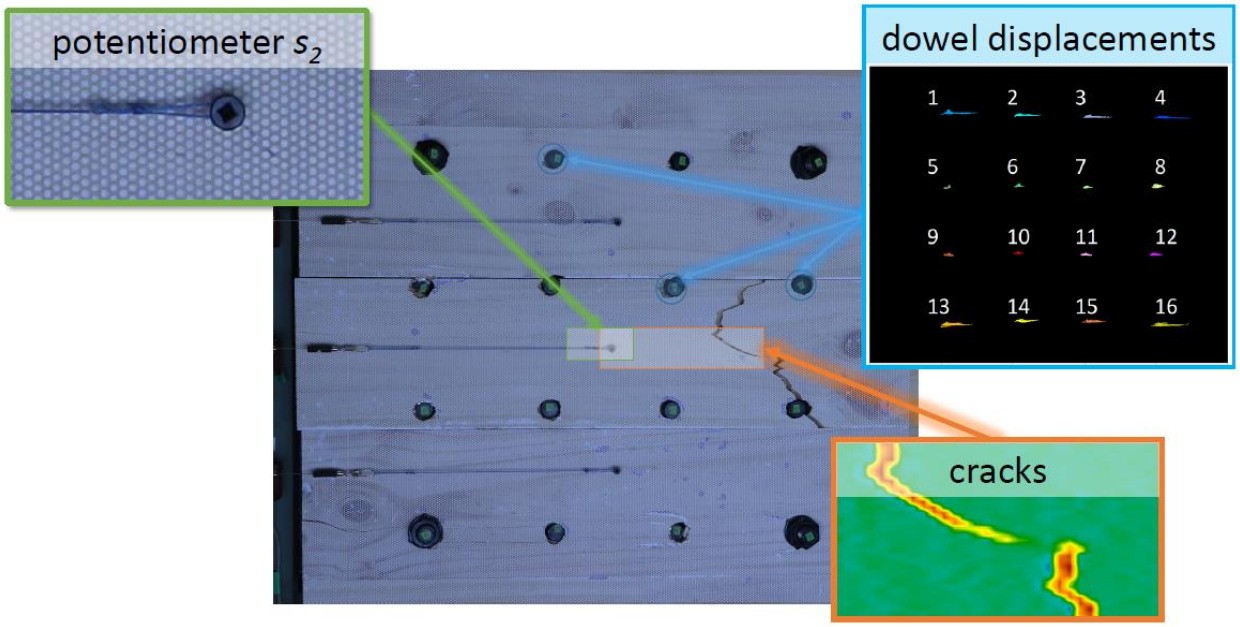

Fig. 9 Different PTV analyses based on same captured image.

3.2.1 Potentiometer displacement vs measuring point

In order to assess PTV accuracy, the displacements of a potentiometer string attachment point (measuring point s_k in Figure 2a) were computed by means of PTV and compared to the corresponding potentiometer readings. As a set of reference particles was applied to each potentiometer mount, it was possible to calculate the relative displacement vector between the string attachment point and potentiometer mount, $\boldsymbol{s_k}$*, as given in Equation 7. This was repeated for all 6 potentiometers. Figure 10a displays the average potentiometer readings, average PTV displacements of the measuring points as well as the difference between the two. It can be seen that the readings differ the most at the start of a load cycle. This is likely due to a rigid body rotation of the CLT panel during loading and unloading (Ottenhaus et al. 2018). In order to overcome friction between the panel and the roller support, the top jack had to slightly lift up the panel at the start of each load cycle resulting in a small rotation around the support frame where the potentiometers were mounted. This behaviour is also reflected in the difference between the jack forces in Figure 10b: the top jack applied significantly higher load in each loading and unloading cycle with an additional lag between top and bottom jack in each loading cycle.

As string potentiometers only register string elongation, these rigid body rotations were not recorded by the potentiometers but registered as a net positive displacement in the x-direction by PTV as well as residual x-displacements from t = 1000 s onwards. For the large-scale connection testing, the panel rotations had little impact on the final test results in terms of load at failure, ultimate displacement, ductility, and energy dissipation. It should be noted that only after a complete PTV analysis had been conducted, was it possible to confirm that the connections were predominantly subjected to one-directional loading in the intended loading direction. However, there may be experimental setups or practice applications where these unexpected behaviours have a significant impact on the test results. In those cases, traditional measuring techniques may produce inaccurate results and it may also not be possible

to detect this inaccuracy. PTV on the other hand is able to produce accurate results regardless of the specimen's response provided that there is no significant out-of-plane motion.

$$\boldsymbol{s_k^*} = \boldsymbol{s_k} - \boldsymbol{d_{ref}}; k = 1 \dots 6$$

$$PTV\ displacement = \frac{1}{6}\sum_{k=1}^{6} \begin{cases} \|s_k^*\| & s_{kx}^* \geq 0 \\ -\|s_k^*\| & s_{kx}^* < 0 \end{cases} \quad (7)$$

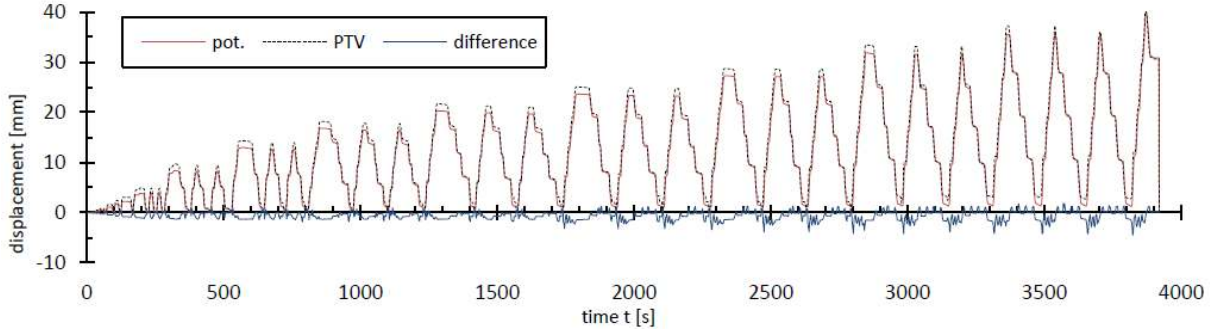

(a)

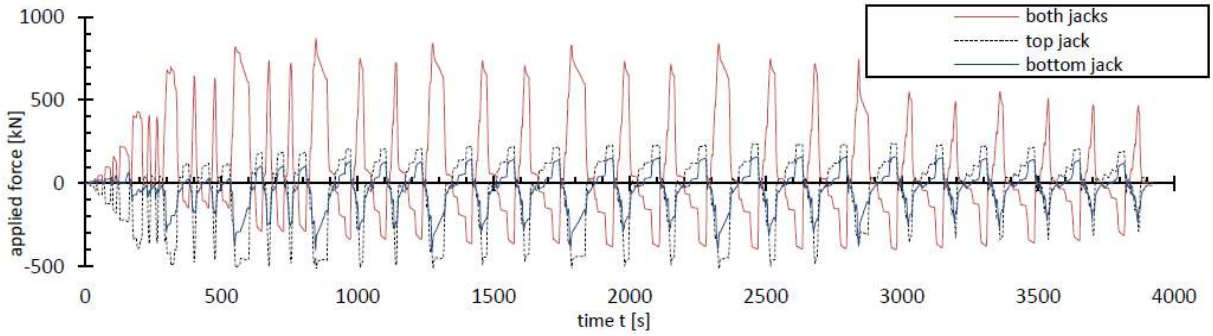

(b)

Fig. 10 a) Potentiometer readings and PTV displacements of measuring points, b) force applied by hydraulic jacks.

3.2.2 Dowel displacement

The dowel displacements were computed for each time step *t* by tracking the green dowel labels by means of PTV. Note that the connection displayed in Figure 11 was loaded at the left hand side of the image. The images were thus taken at the opposite side of the test setup displayed in Figure 2b. Figure 11a shows an overlay of the resulting particle paths on the captured image at *t* = 1798 s. Figure 11b shows the identical paths with colour coding and labelling of the dowels. The same colour coding is used in Figure 11c which displays the dowels' x-positions versus time. The grey line shows the average loading jack displacement versus time. It can be clearly seen that a vertical crack formed shortly after *t* = 700 s between dowel 8 and 12 after which dowels 5-12 experienced a phase lag with much smaller displacements than the top and bottom row of dowels. It can also be seen that there was residual displacement and plastic deformation in all dowels.

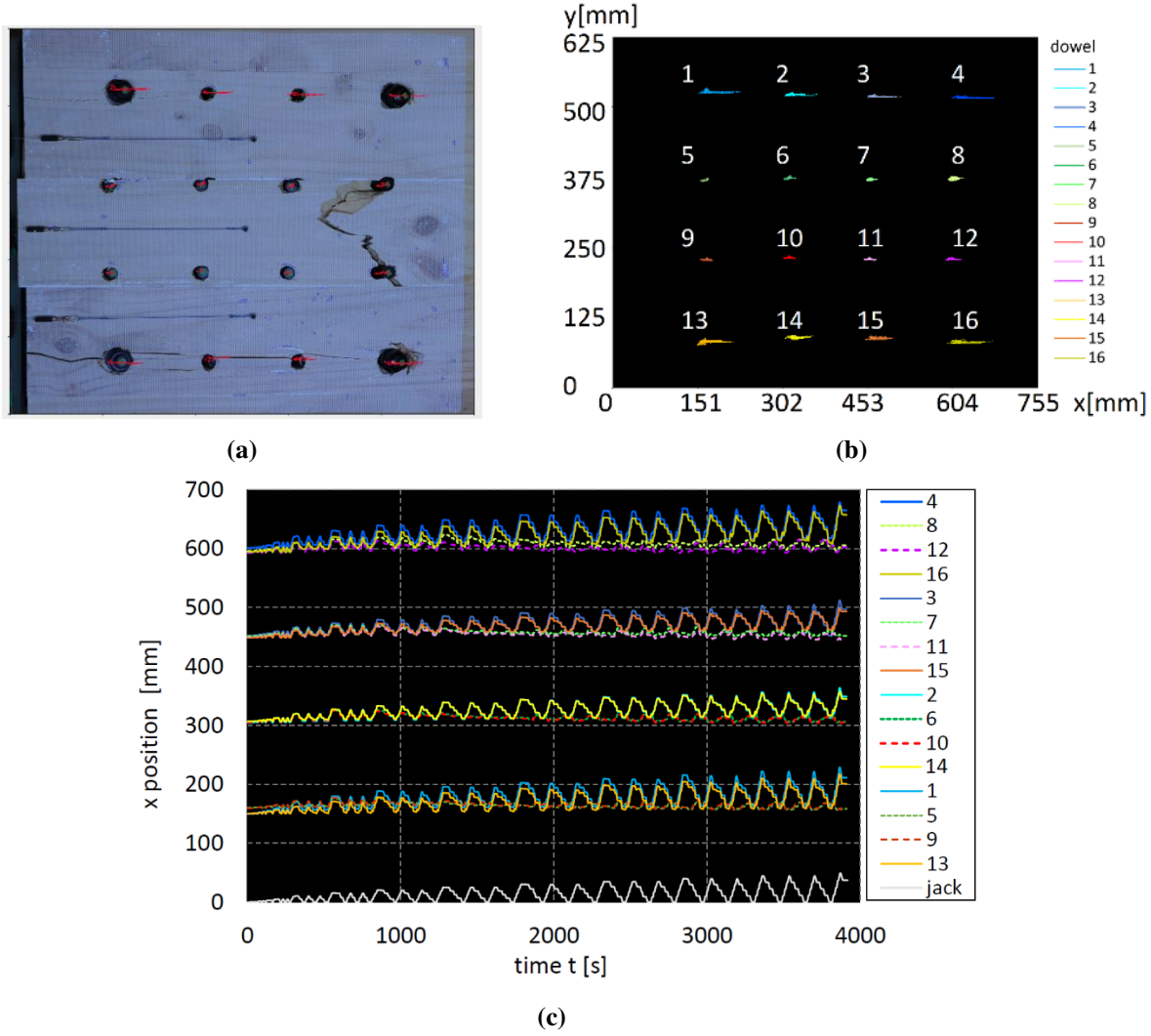

Fig. 11 Dowel positions: a) particle path overlay on fractured connection, b) colour coded particle paths, c) dowel and average jack x-position vs time.

Figure 12 displays the x-displacements for individual rows of dowels as well as the average jack displacement. It can be seen from Figure 12a and 12d that in the top and bottom row, the dowels located furthest from the panel edge (dowel 4 and 16) experienced the highest displacements followed by the dowels closest to the panel edge (dowels 1 and 13). This behaviour is expected as these dowels in the corners (1, 4, 13, 16) had threaded ends with hand-tight nuts and washers and thus experienced some rope effect during plastic deformation. Furthermore, dowels 1-4 and 13-16 experienced significant plastic deformation and residual displacement as their displacements did not return to zero, whereas the jack displacements returned to zero displacement in each load cycle. After subtraction of this residual displacement, there is still a difference of up to 10 mm between the peak displacements of the dowels and the peak displacements of the jacks. This is owed to the plastic deformation of the dowels which caused a rotation of the dowel heads which was most pronounced for dowels 4 and 16 and can be seen in Figure 11a.

Figure 12b and 12c display the x-displacements for the inner dowel rows (5-8 and 9-12). As expected in typical dowelled connections with multiple dowels, the dowels furthest from the edge (8 and 12) experienced the highest x-displacements, followed by those dowels located closer to the edge (7 and 11, then 6 and 10), with those dowels located closest to the edge experiencing the smallest displacements (5 and 9). This behaviour changed once a crack had been formed between dowels 8 and 12 after which the dowel displacements were much smaller than the jack displacements. Overall, PTV provided an excellent tool for contact-free measurements of dowel displacements in this experiment.

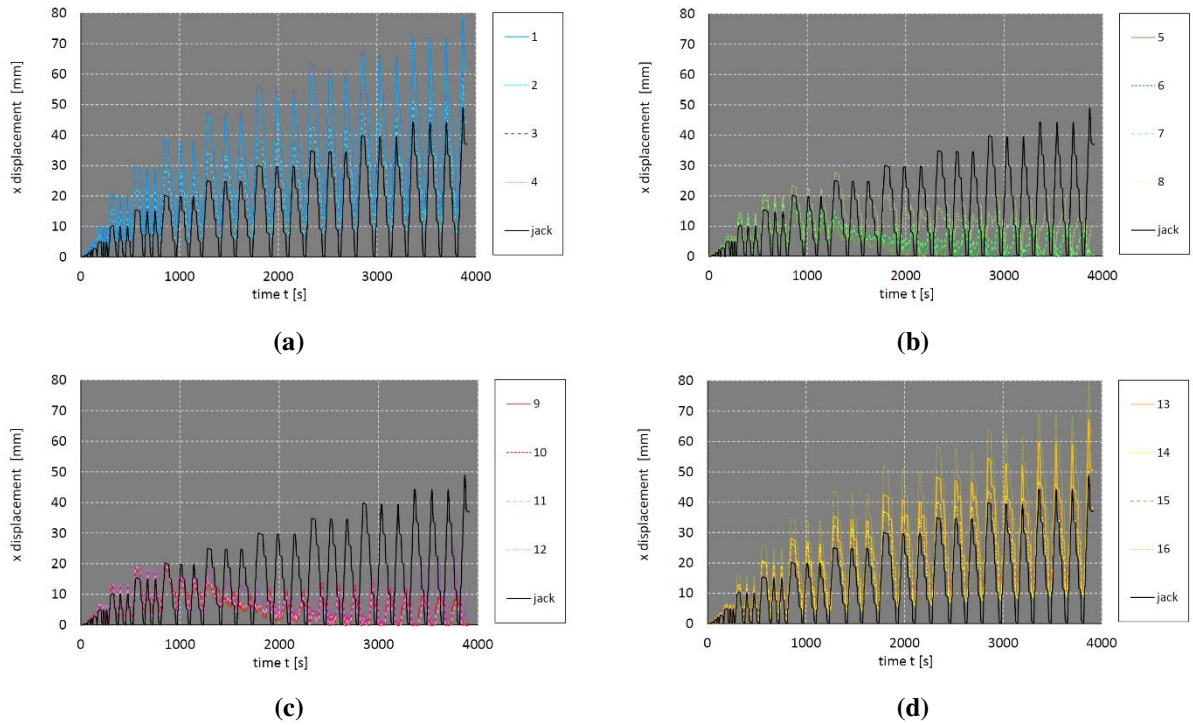

Fig. 12 Dowel and jack x-displacements vs time: a) dowels 1-4, b) dowels 5-8, c) dowels 9-12, d) dowels 13-16.

3.2.3 Crack growth

The white background particles to the right of the potentiometer measuring point s_2 (Figure 2a) between dowel 8 and 12 were tracked by means of PTV. Figure 13 displays the displacement and equivalent ε_{xx} strain fields at the onset of cracking at t = 760 s and t = 848 s. Figure 13a and 13c show that the area to the right of the crack experienced much higher x-displacements than the area to the left of the crack. This was in agreement with the dowel displacements. Figure 13b and 13d show that the cracked zone exhibited positive strain in the x-direction which indicates tension parallel to the grain, whereas there was negative strain just left of the crack, indicating compression. The latter is an effect of unloading where the panel was pushed back towards its initial position until the loading jacks registered zero displacement. It should be noted that due to the particle triangulation the equivalent surface strain in Figure 13b and 13d was interpolated over the crack width and has therefore no physical meaning in the cracked zone itself. However, the equivalent strain results are indicative of the crack location, growth direction, and size.

PTV also provided a good tool to measure the entire displacement field around the crack, whereas the potentiometer s_2 only recorded displacements to the left of the crack. It is generally difficult to predict where cracks occur in large-scale timber connections made of complex materials such as CLT, and it is also hard to measure strain fields of timber materials with conventional strain gauges. In contrast, in this experiment, PTV was able to monitor crack growth in a contact-free manner without prior knowledge of the crack location. Using PTV, there is no limitation to the direction or size of the crack growth, or the number of cracks. Furthermore, it is possible to compute cumulative strain for individual load cycles or between individual time steps.

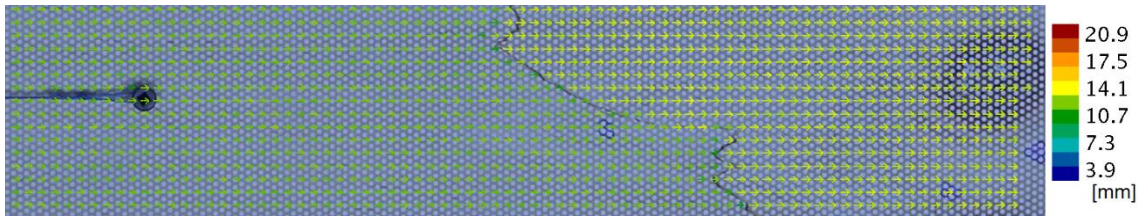

(a)

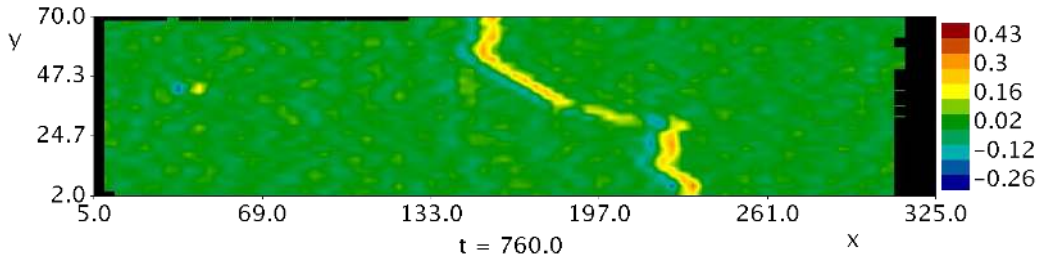

(b)

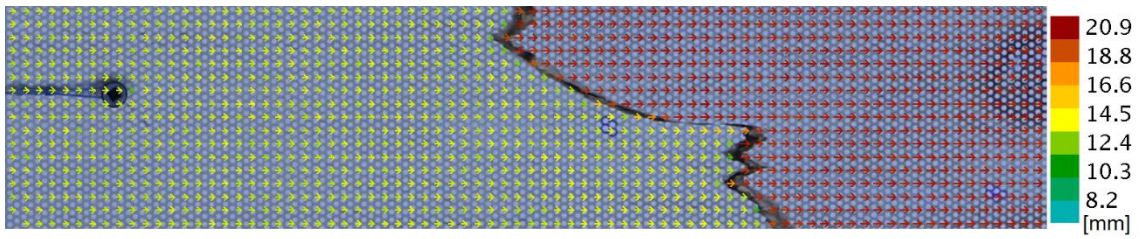

(c)

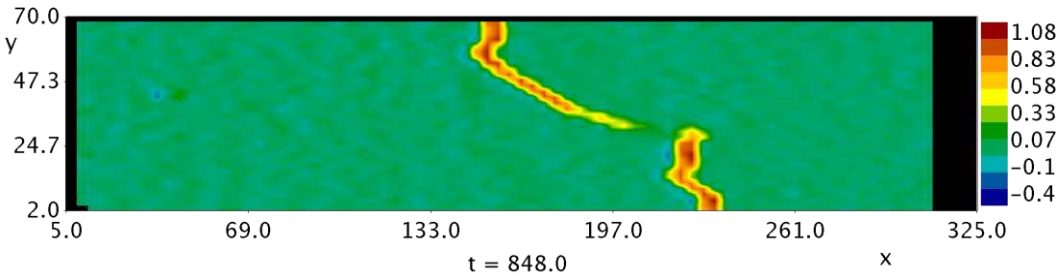

(d)

Fig. 13 Crack growth: a) displacement field at t = 760 s, b) equivalent cumulative ε_{xx} strain from t = 728...760 s, c) displacement field at t = 848 s, d) equivalent cumulative ε_{xx} strain from t = 820...848 s.

3.3 SMALL CLEAR SPECIMENS

ASTM D143-09 requires recording of the load at failure and sketching of the final failure. Not only does PTV capture the sample at failure, it also makes it possible to gain information about the strain field leading up to failure. It should be noted that once surface cracking occurs, the equivalent cumulative surface strain interpolated over the crack width has no physical meaning. However, the obtained equivalent strain field can serve as an indication of the crack tip, crack size, and growth direction e.g. in a qualitative comparison to FEM results.

Figure 14a displays the failure and Figure 14b displays the load displacement curve and PTV results of a sample of *radiata pine* LVL. From the load displacement curve in Figure 14b it can be seen that the sample failed in a brittle manner and hardly any shear strain was detected prior to failure at t = 150.5 s. The plastic shear strain γ_{xy} was captured well by PTV and although some PTV particles were located on the failure plane and thus not matched, the crack is clearly visible at t = 157.5 s.

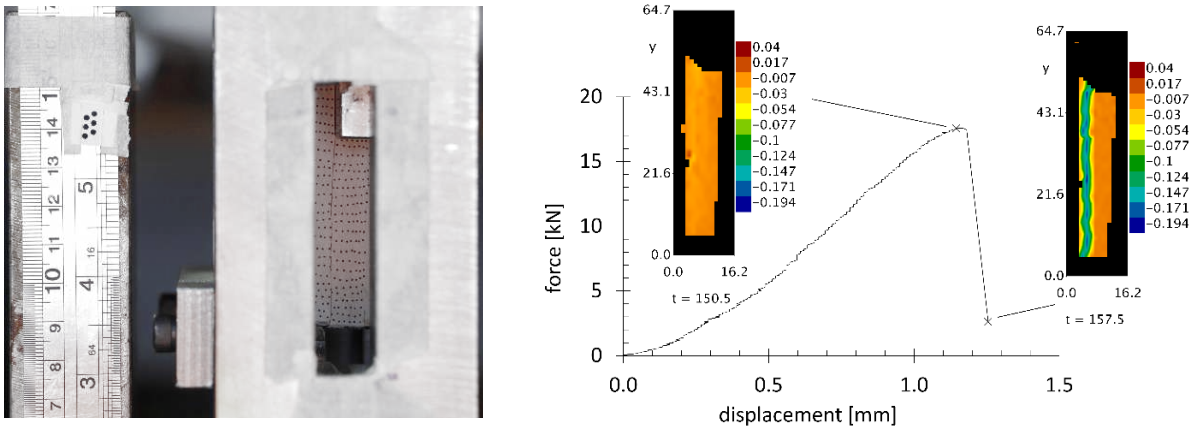

(a) **(b)**

Fig. 14 Shear test in LVL: a) test setup and crack at failure, b) load displacement curve and equivalent cumulative shear strain γ_{xy}.

Figures 15a and 15b display the results of a small clear sample of *radiata pine* loaded in tension perpendicular to the grain. This sample failed in a brittle manner at t = 35.0 s. As can be seen in Figure 15b, strain concentrations of $\varepsilon_{yy} \approx$ 0.12 had accumulated at this point in the lower half of the reduced cross section. In the subsequent time step, t = 35.5 s a crack had grown through the entire cross section, leading to a cumulative strain of $\varepsilon_{yy} \approx 0.23$ in the cracked zone. This crack was then further opened as the crack propagated through the depth of the specimen until the experiment was terminated at t = 50.5 s.

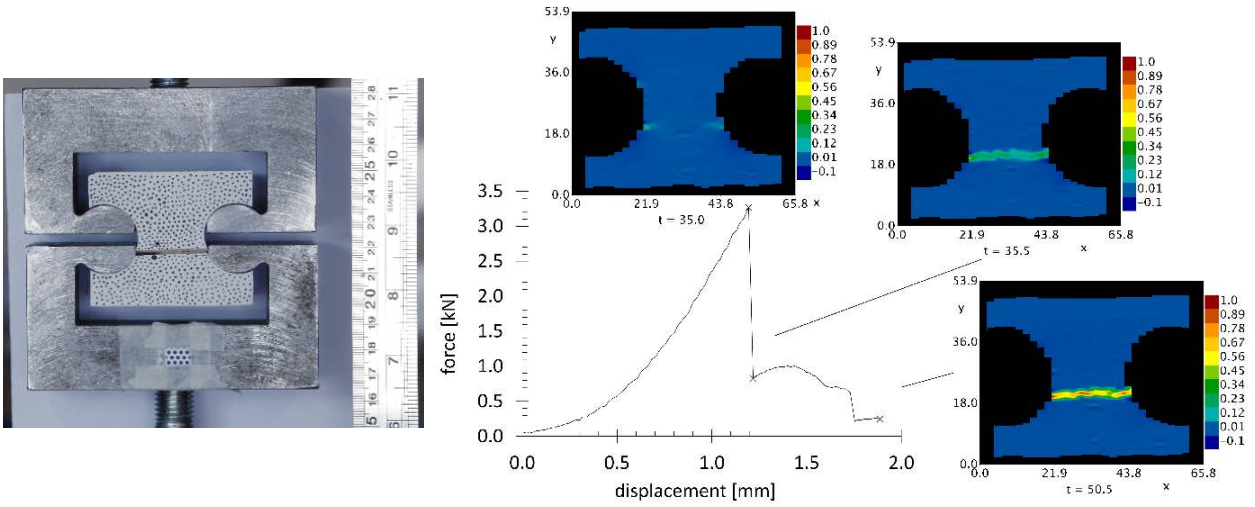

(a) **(b)**

Fig. 15 Tension perpendicular to the grain in clear *radiata pine*: a) test setup and crack at failure, b) load displacement curve and equivalent cumulative strain ε_{yy}.

Figures 16a and 16b display the results of a cleavage test in *radiata pine*. Unlike the shear and tension parallel to the grain specimens this specimen failed in a more ductile manner. Cumulative strain concentrations of $\varepsilon_{yy} \approx 0.08$ can be seen prior to failure at $t = 56.0$ s indicating the development of a crack. At $t = 66.0$ s, the specimen started to fail with cumulative strains reaching up to $\varepsilon_{yy} \approx 0.54$ at the crack root. At $t = 94.5$ s the crack had grown through most of the specimen and the experiment was terminated. In all three small clear test setups, PTV was able to capture the elastic and plastic strain without requiring prior knowledge of the location of the crack growth.

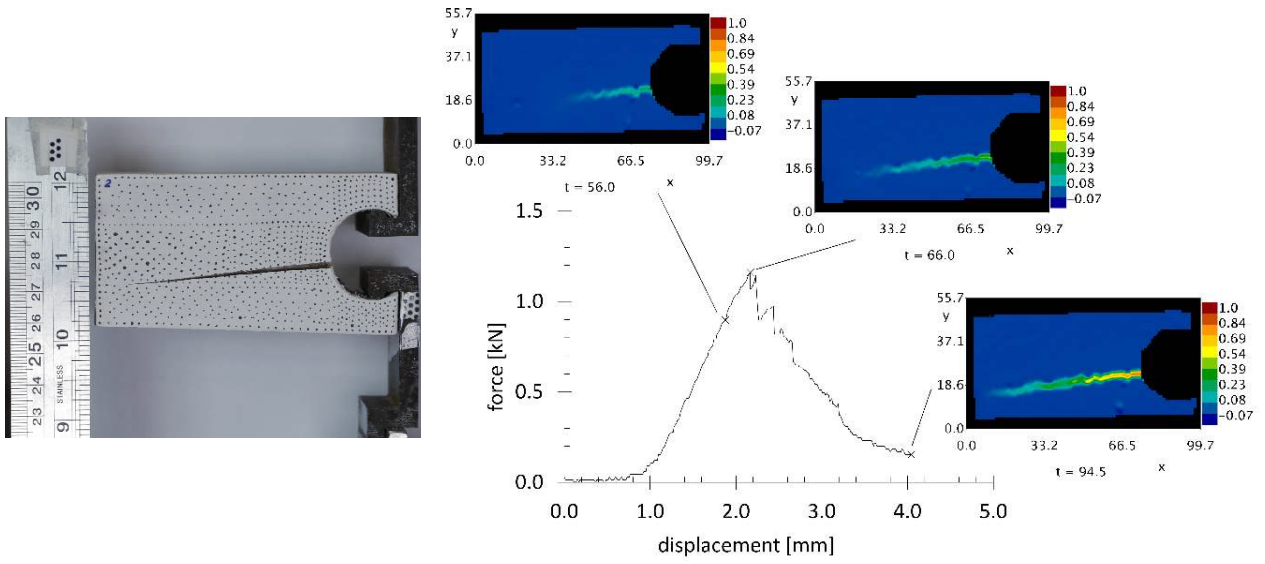

(a) **(b)**

Fig. 16 Cleavage test in clear *radiata pine*: a) test setup and crack at failure, b) load displacement curve and equivalent cumulative strain ε_{yy}.

4 CONCLUSIONS

The methodology and application of Particle Tracking Velocimetry (PTV) in structural timber engineering has been discussed in this paper for the examples of embedment tests, large-scale connection tests, and small clear material tests. It was demonstrated that PTV was able to accurately measure fastener displacements in large-scale connection tests, while simultaneously monitoring crack growth in the timber substrate. Furthermore, the accuracy of the PTV method was assessed by comparing potentiometer measurements to PTV results of the same measuring points. It was found that PTV improved the data accuracy, as it was capable of detecting the unanticipated CLT panel rotations in large-scale connection tests, as well as movements perpendicular to the loading direction, i.e. crack opening in dowel embedment tests. These phenomena cannot be detected by conventional measuring techniques.

Another advantage of PTV is its contact-free nature because it does not interfere with specimen behaviour. Conventional measuring devices often require alteration of the specimen, e.g. through drilling of holes to attach potentiometers / LVDTs or though application of strain gauges, which can affect the specimen's response. Furthermore, these devices only record information from a very limited number of measuring points, whereas the number of measuring points in PTV is only limited by the number of applied particles and image resolution. This can save time for experimental setup, as one single camera with high resolution can replace hundreds of conventional measuring devices. Additionally, the PTV scale can be easily adjusted by using a DSLR camera's zoom function provided a reference scale is captured in the image, whereas conventional measuring devices require calibration and are limited by their maximum displacement or strain range.

On the other hand, PTV requires image post-processing and more intensive data analysis than conventional methods, and is therefore most suited for applications that require contact-free measurements, setups with a large number of measuring points, setups that require high resolution measurements, or in cases where information about the displacement or strain field is desired.

In conclusion, PTV can provide a robust displacement/strain measuring tool in timber engineering research and is able to provide higher data quality and quantity with comparatively little effort at acceptable computational cost while significantly decreasing experimental setup time.

REFERENCES

Adrian, R. J.: Twenty years of particle image velocimetry. *Experiments in Fluids*, *39*(2), 159–169, 2005.

ASTM D143-09, Standard Test Methods for Small Clear Specimens of Timber, *ASTM International*, West Conshohocken, PA, 2009

ASTM D5764 - 97a, Standard Test Method for Evaluating Dowel-Bearing Strength of Wood and Wood-Based Products. *ASTM International*, West Conshohocken, PA, 2013.

Bretagne, N., Valle, V., & Dupré, J. C. (2005). Development of the marks tracking technique for strain field and volume variation measurements. *NDT and E International*, 38(4), 290–298.

Campagnol, J., Radice, A., & Nokes, R.: Lagrangian analysis of bed-load sediment motion: database contribution. *Journal of Hydraulic Research*, *1686*(November), 37–41, 2013.

Chean, V., Robin, E., El Abdi, R., Sangleboeuf, J. C., & Houizot, P.: Use of the mark-tracking method for optical fiber characterization. *Optics and Laser Technology*, *43*(7), 1172–1178, 2011.

Chenouard, N., Smal, I., de Chaumont, F., Maška, M., Sbalzarini, I. F., Gong, Y., Meijering, E.: Objective comparison of particle tracking methods. *Nature Methods*, *11*(3), 281–289, 2014.

Choi, D., Thorpe, J. L., & Hanna, R. B.: Image analysis to measure strain in wood and paper. *Wood Science and Technology*, *25*(4), 251–262, 1991.

Cline, A. K., & Renka, R. L.: A storage-efficient method for construction of a Thiessen triangulation, *Rocky Mountain Journal of Mathematics*, 14, No. 1, pp 119-139, 1984.

Crowe, A, Davidson, M.,and Nokes, R. Velocity measurements in inclined negatively buoyant jets, *Environmental Fluid Mechanics*, 16, 3, pp503-520, 2016.

Dubois, F., Méité, M., Pop, O., & Absi, J.: Characterization of timber fracture using the Digital Image Correlation technique and Finite Element Method. *Engineering Fracture Mechanics*, *96*, 107–121, 2012.

Henke, K., Pawlowski, R., Schregle, P., & Winter, S. Use of digital image processing in the monitoring of deformations in building structures. *Journal of Civil Structural Health Monitoring*, *5*(2), 141–152, 2015.

McCormick, N., & Lord, J.: Digital image correlation. *Materials Today*, *13*(12), 52–54, 2010.

Mokhtari, M., Hayatdavoudi, A., Nizamutdinov, R., Rizvi, H., & Nath, F. Characterization of Complex Fracture Propagation in Naturally Fractured Formations Using Digital Image Correlation Technique. *Society of Petroleum Engineers*, 2017

Murata, K., Masuda, M., & Ukyo, S.: Analysis of Strain Distribution of Wood Using Digital Image Correlation Method. *Transaction of the Visualization Society of Japan*, *25*(9), 57–63, 2005.

Nokes, R.: *Streams: System Theory and Design*. 2017

Ottenhaus, L., Li, M., Nokes, R.: Application of Particle Tracking in Large Scale Timber Connection Testing. In *Proceedings of WCTE 2018*, 2018

Ottenhaus, L.-M., Li, M., Smith, T. Ductility of large-scale dowelled CLT connections under monotonic and cyclic loading. *Australian Earthquake Engineering Society 2017 Conference, Canberra, 24-26 Nov 2017*, 2017.

Pan, B., Qian, K., Xie, H., & Asundi, A.: Two-dimensional digital image correlation for in-plane displacement and strain measurement: a review. *Measurement Science and Technology*, *20*(6), 2009.

Papastavrou, P., Smith, S., Wallwork, T., Mcrobie, A., & Niem, N.: Design of Cross-Laminated Timber Slabs with Cut-Back Glulam Rib Downstands, In *Proceedings of WCTE 2016*, 2016.

Pop, O., & Dubois, F.: Determination of timber material fracture parameters using mark tracking method. *Construction and Building Materials*, *102*, 977–984, 2016.

Qiao., J., Delevan, S., Nokes, R., and Plew, D. Flow structure and turbulence characteristics downstream of a spanwise suspended linear array. *Environmental Fluid Mechanics*, 16, 5, pp1021-1041, 2016.

Samarasinghe, S., Kulasiri, D., & Nicolle, K.: *Study of Mode-I and Mixed-Mode Fracture in Wood using Digital Image Correlation Method*. *Engineering*. Lincoln University, 1997.

Sutton, M., Wolters, W., Peters, W., Ranson, W., & McNeill, S.: Determination of displacements using an improved digital correlation method. *Image and Vision Computing*, *1*(3), 133–139, 1983.

van Beerschoten, W. a., Carradine, D. M., & Carr, a.: Development of constitutive model for laminated veneer lumber using digital image correlation technique. *Wood Science and Technology*, *48*(4), 755–772, 2014.

Zhou, J., Cenedese, C., Williams, T., Ball, M., Venayagamoorthy, K., & Nokes, R. I.. On the propagation of gravity currents over and through a submerged array of circular cylinders. *Journal of Fluid Mechanics*, 831, 394-417, 2017.

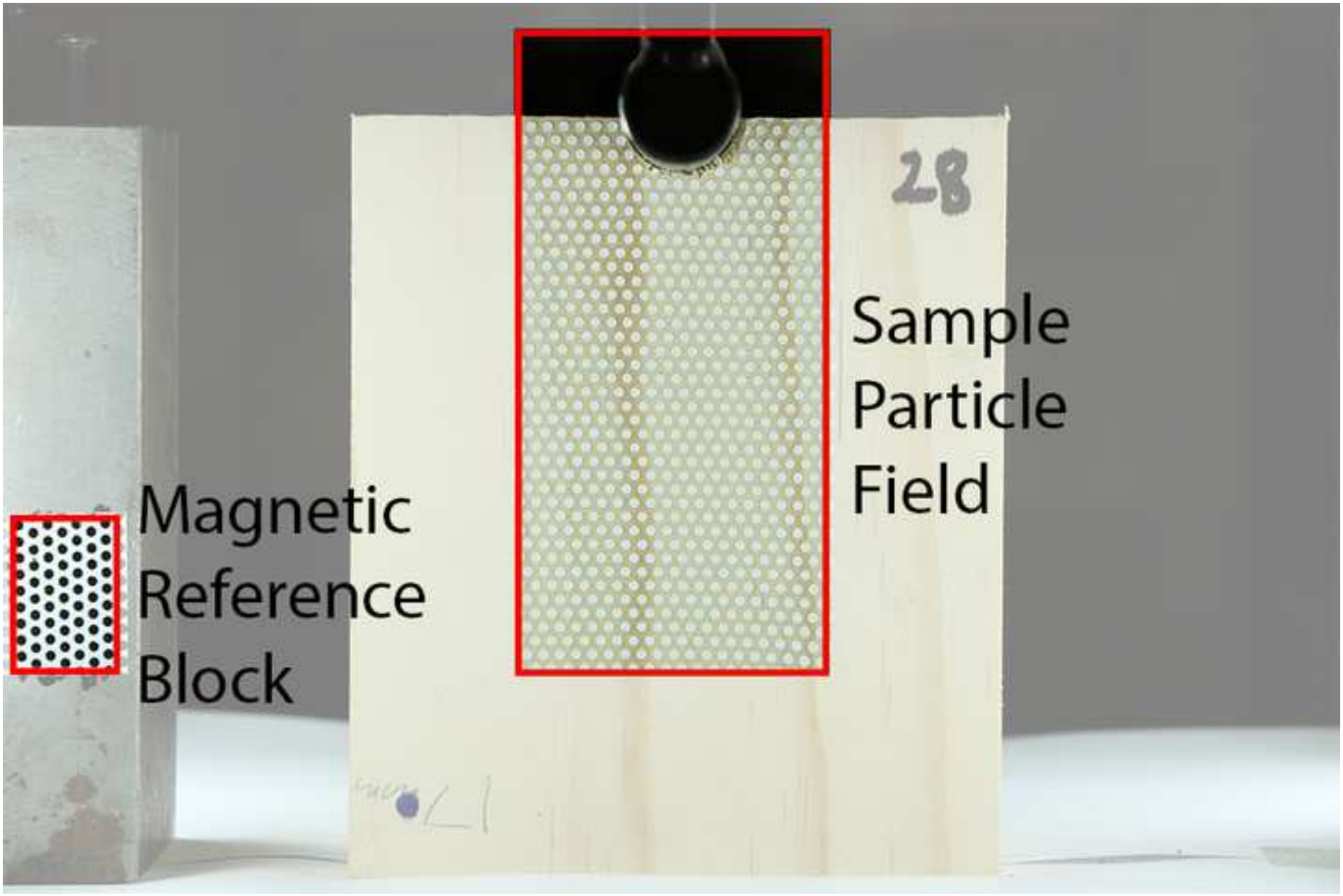

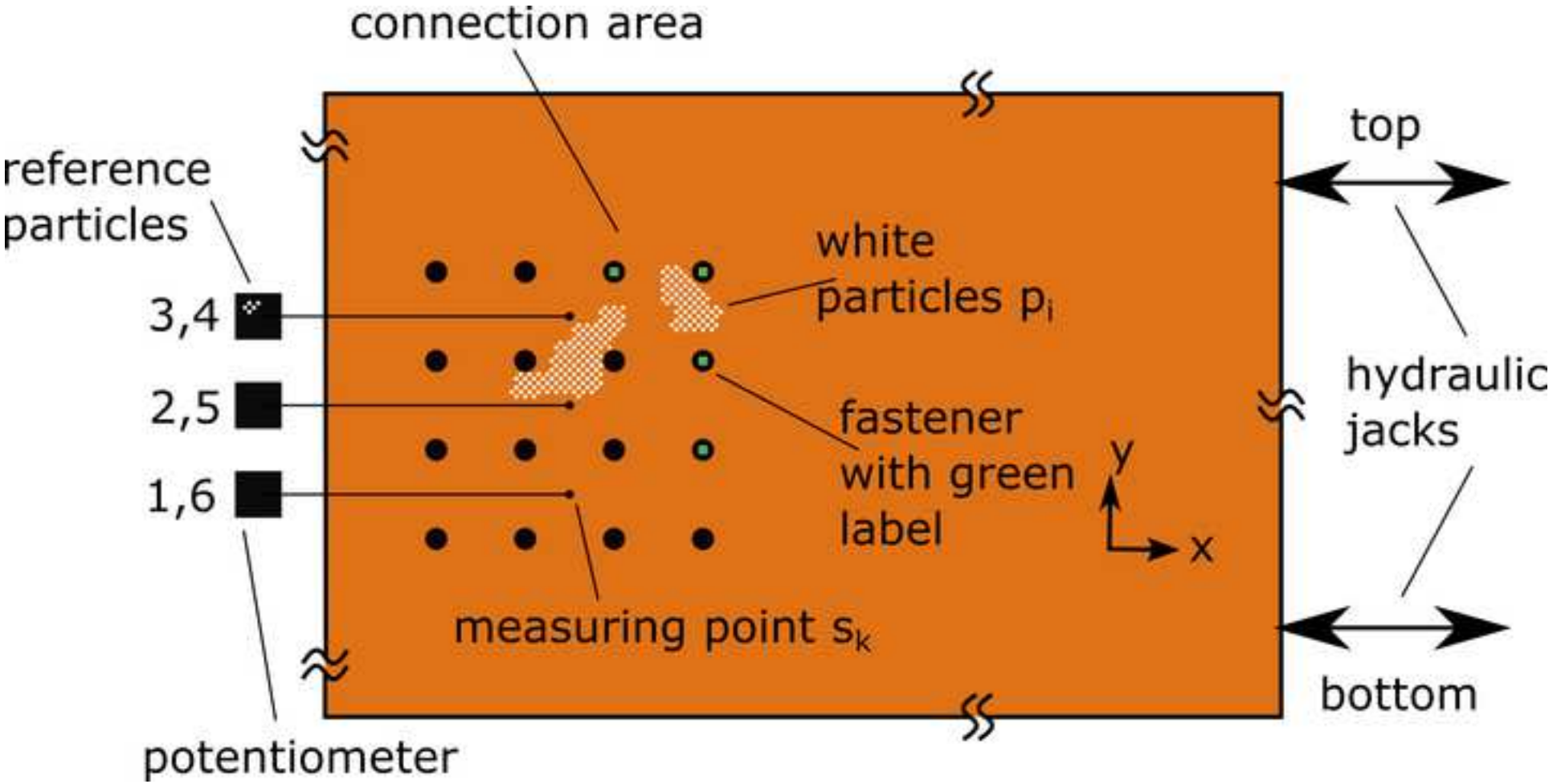

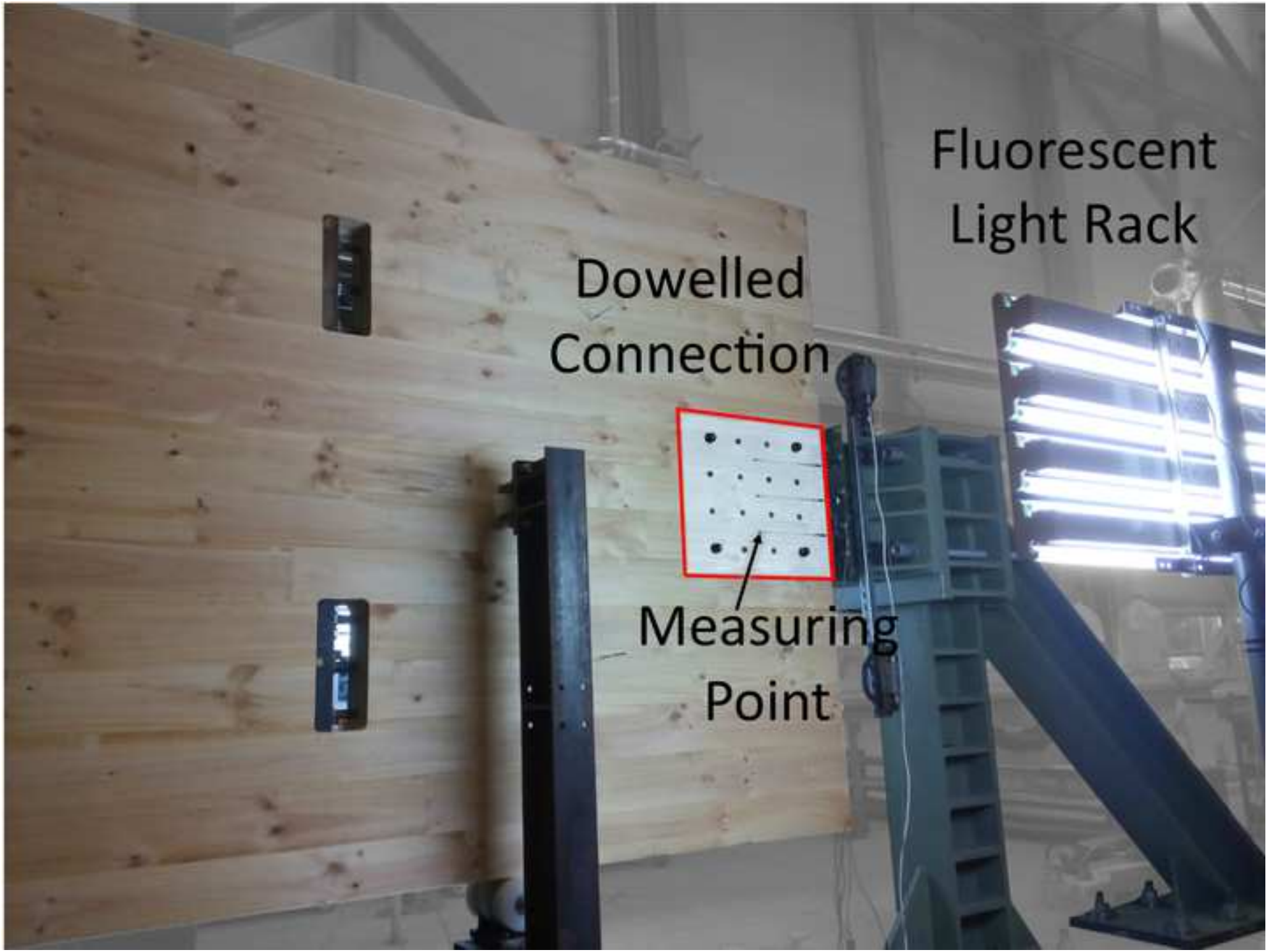

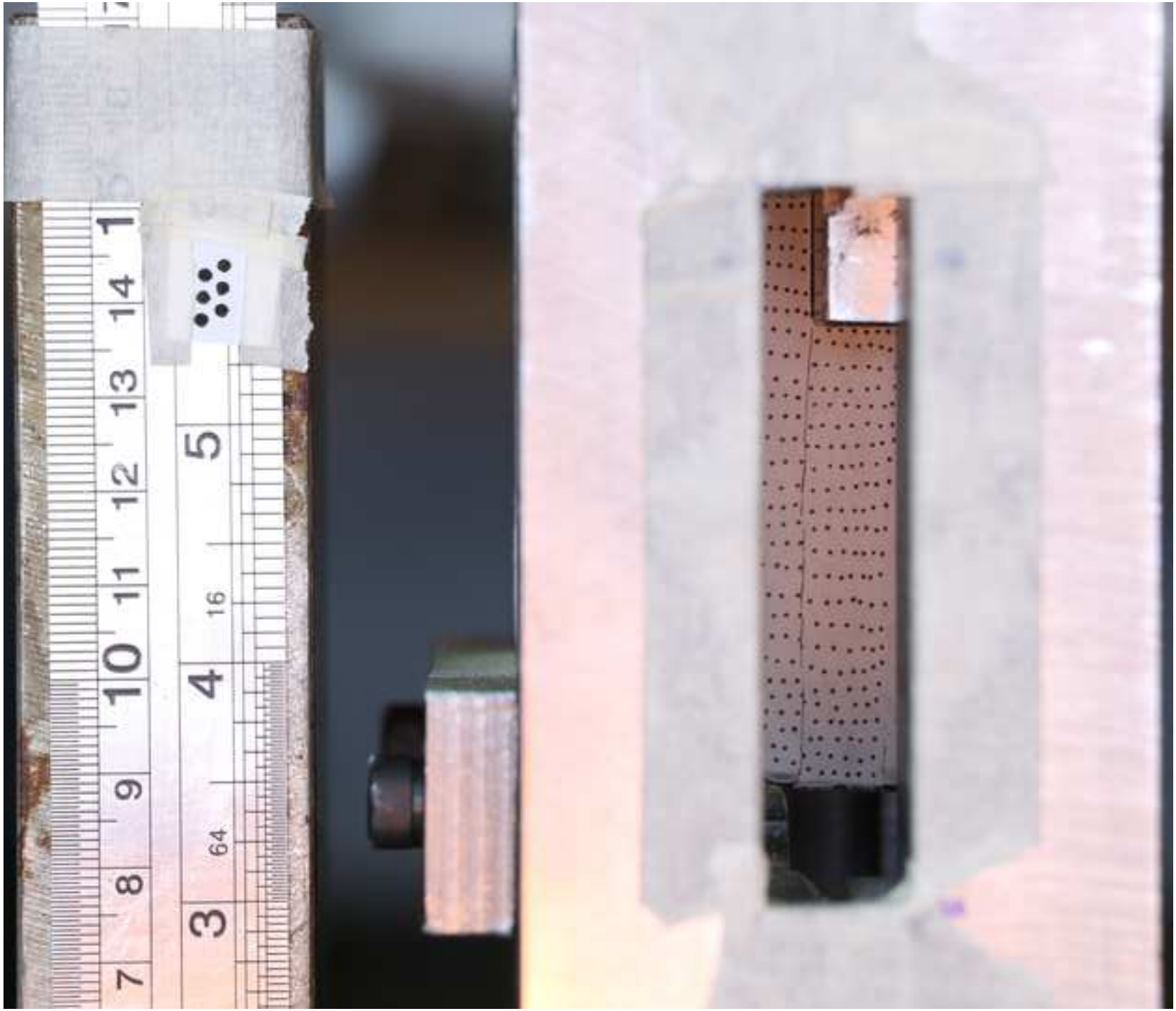

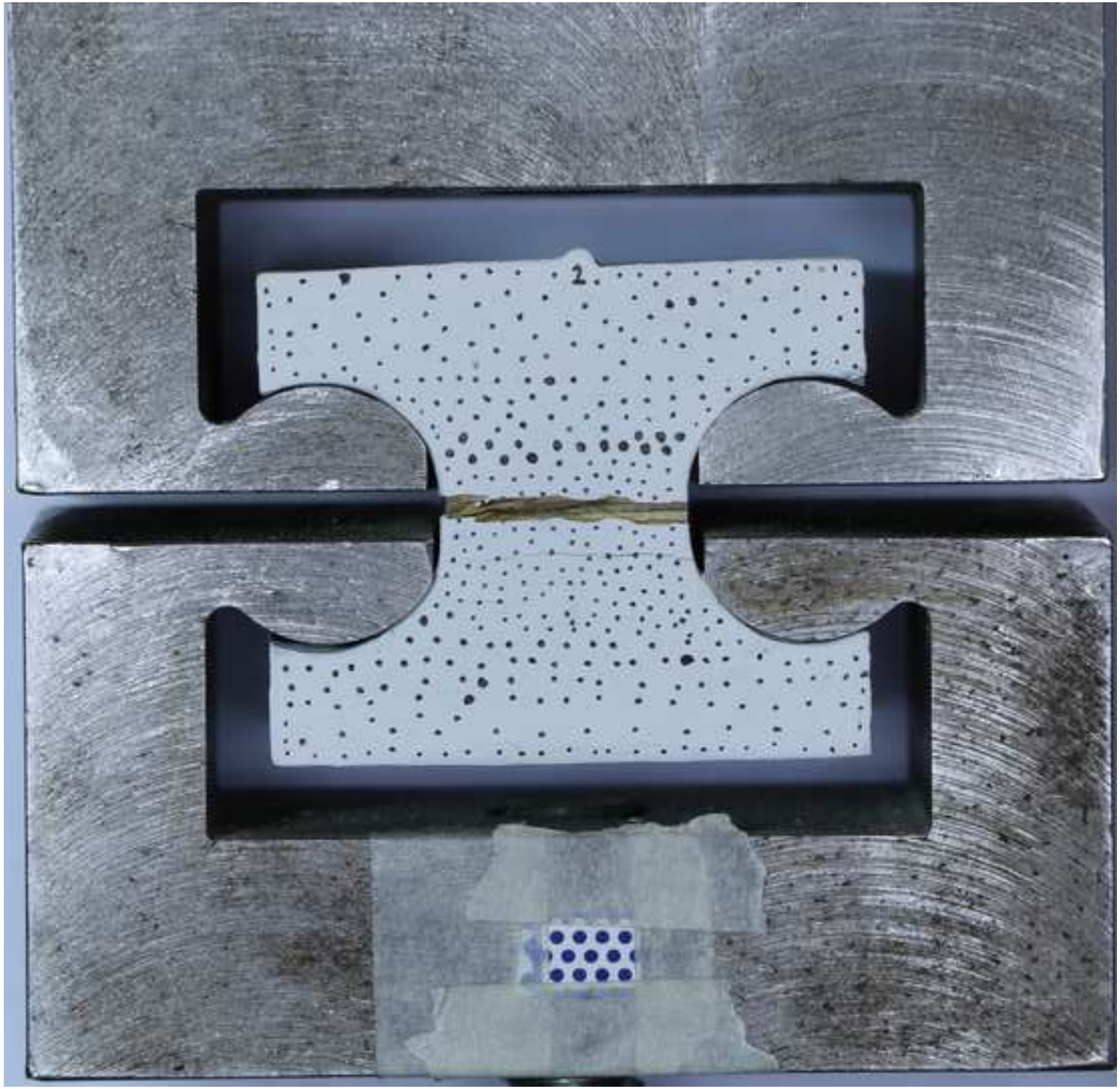

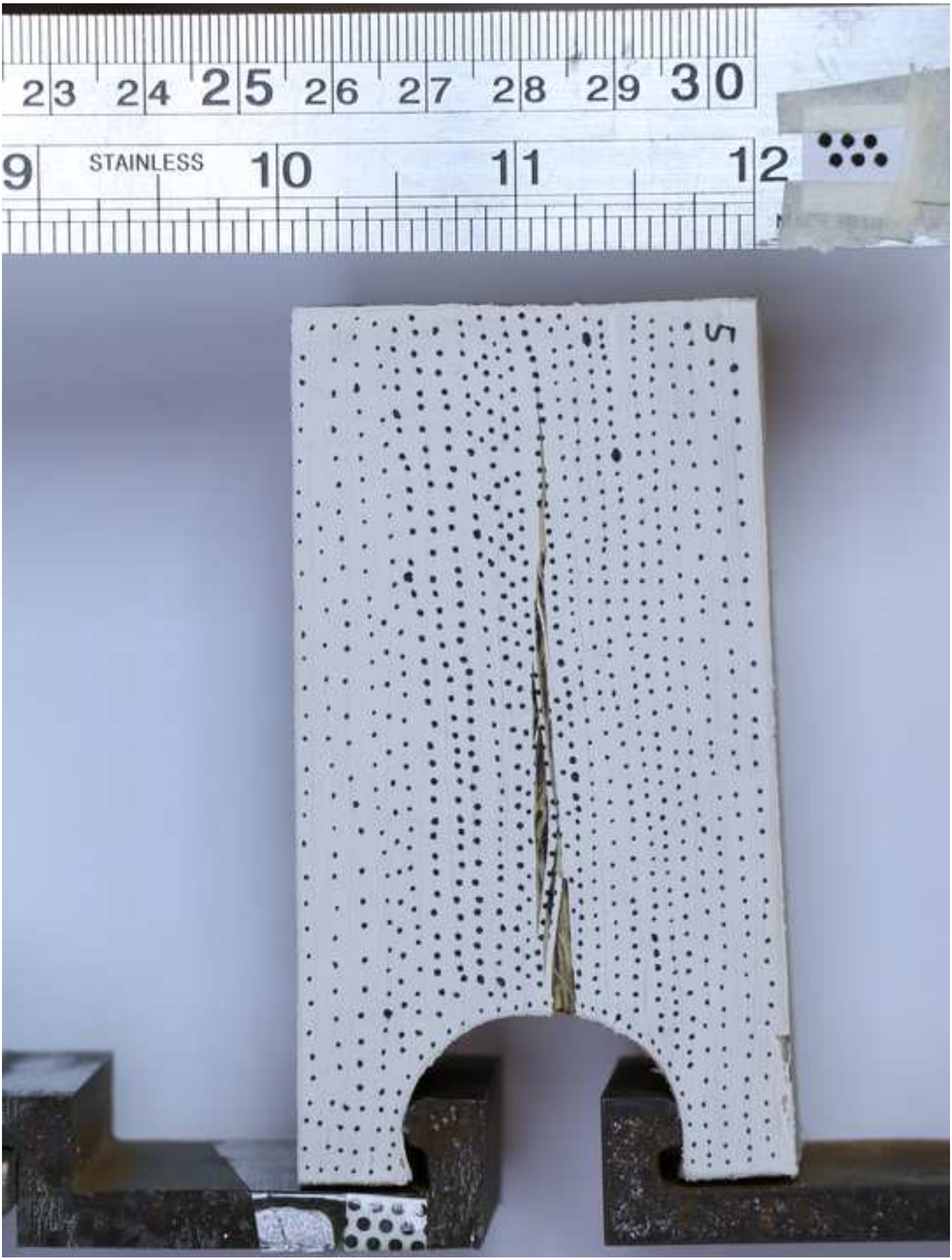

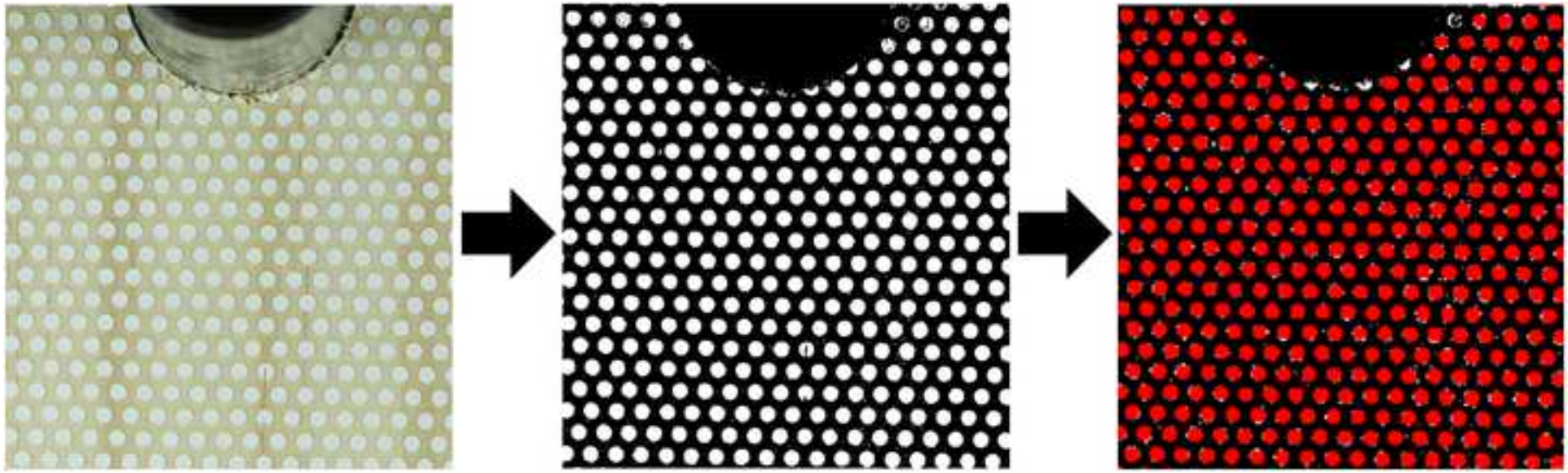

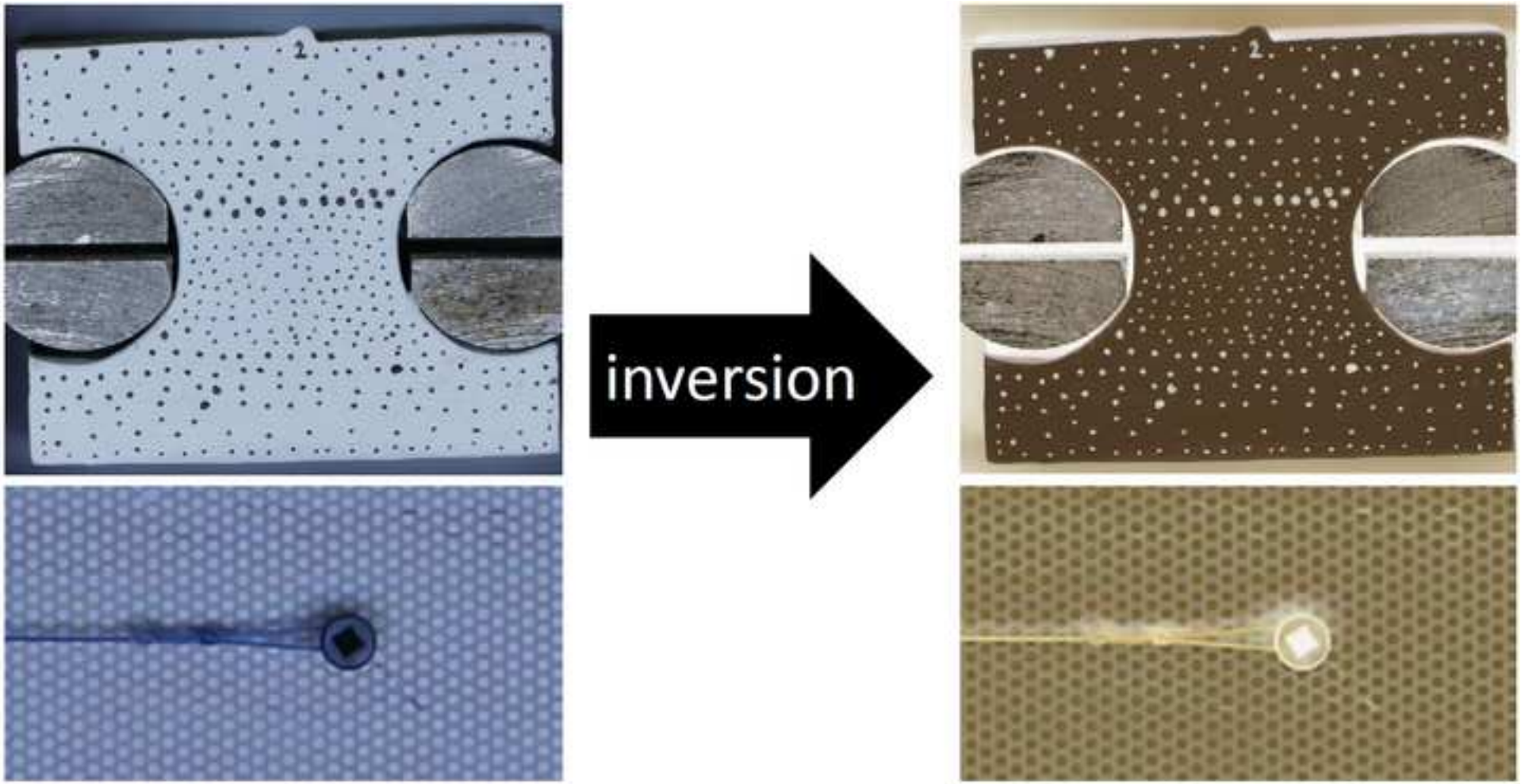

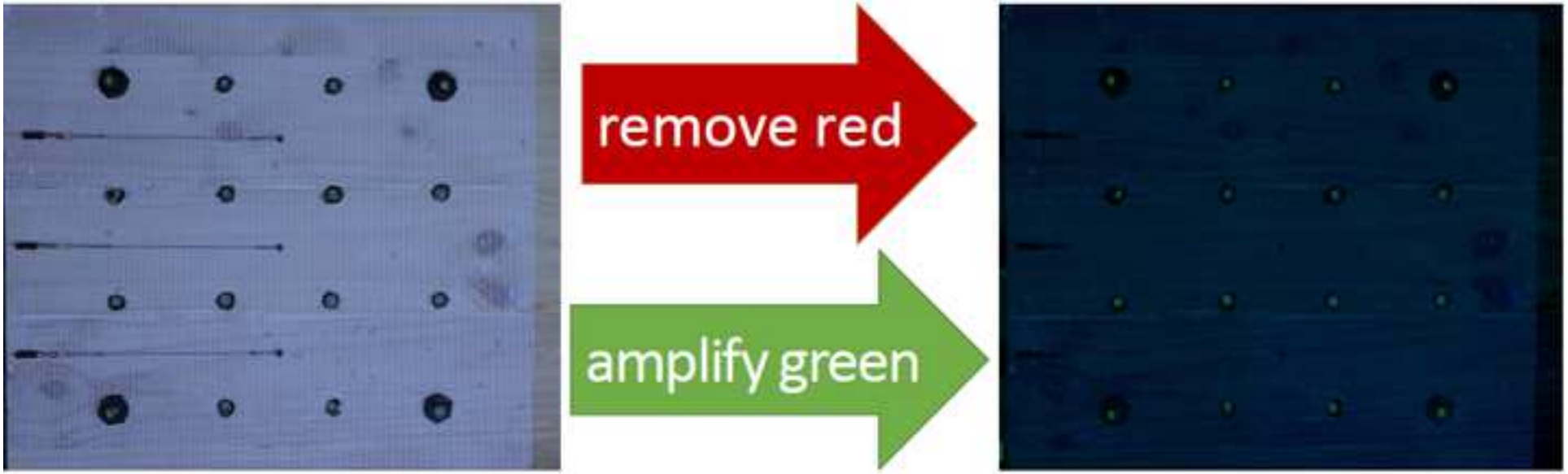

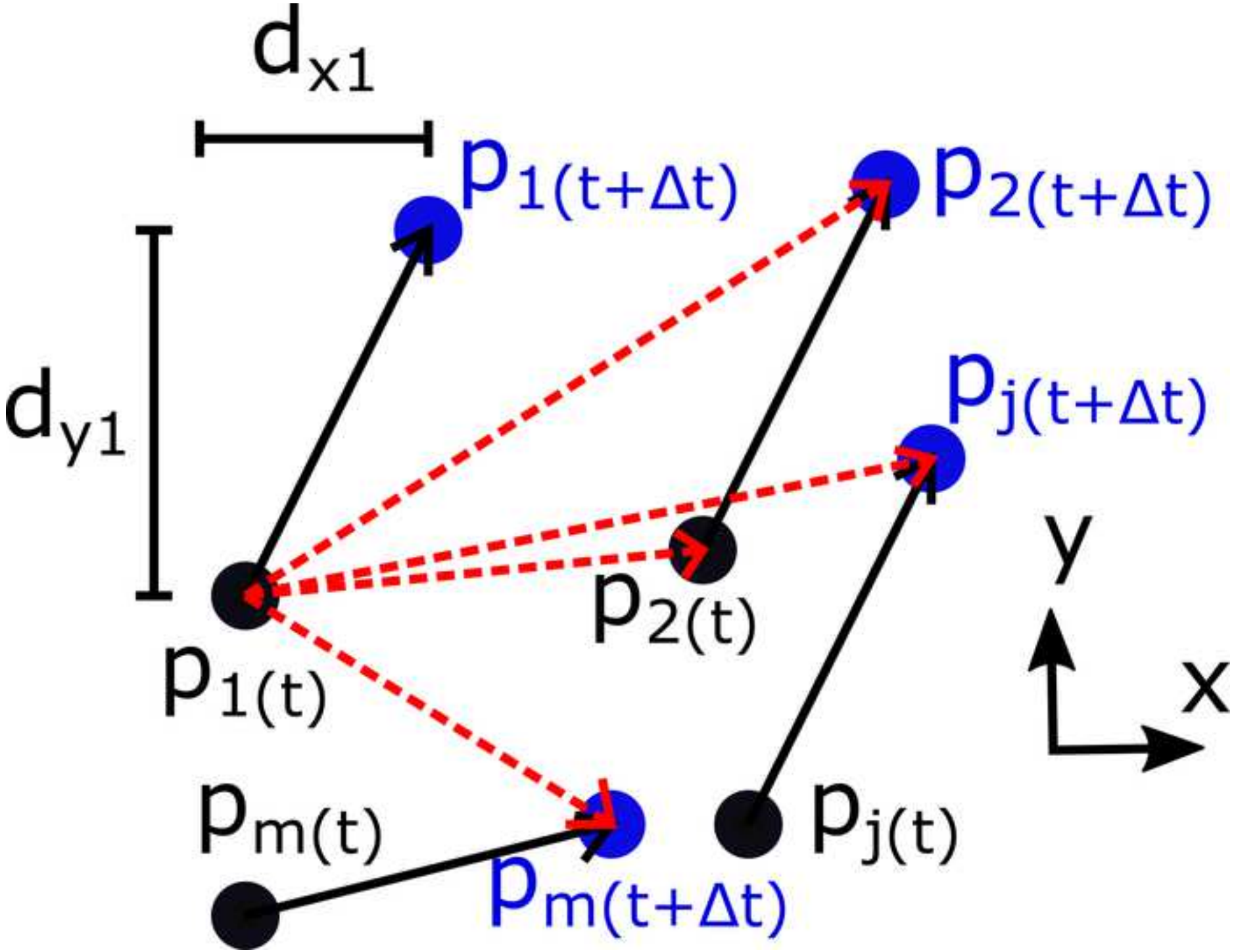

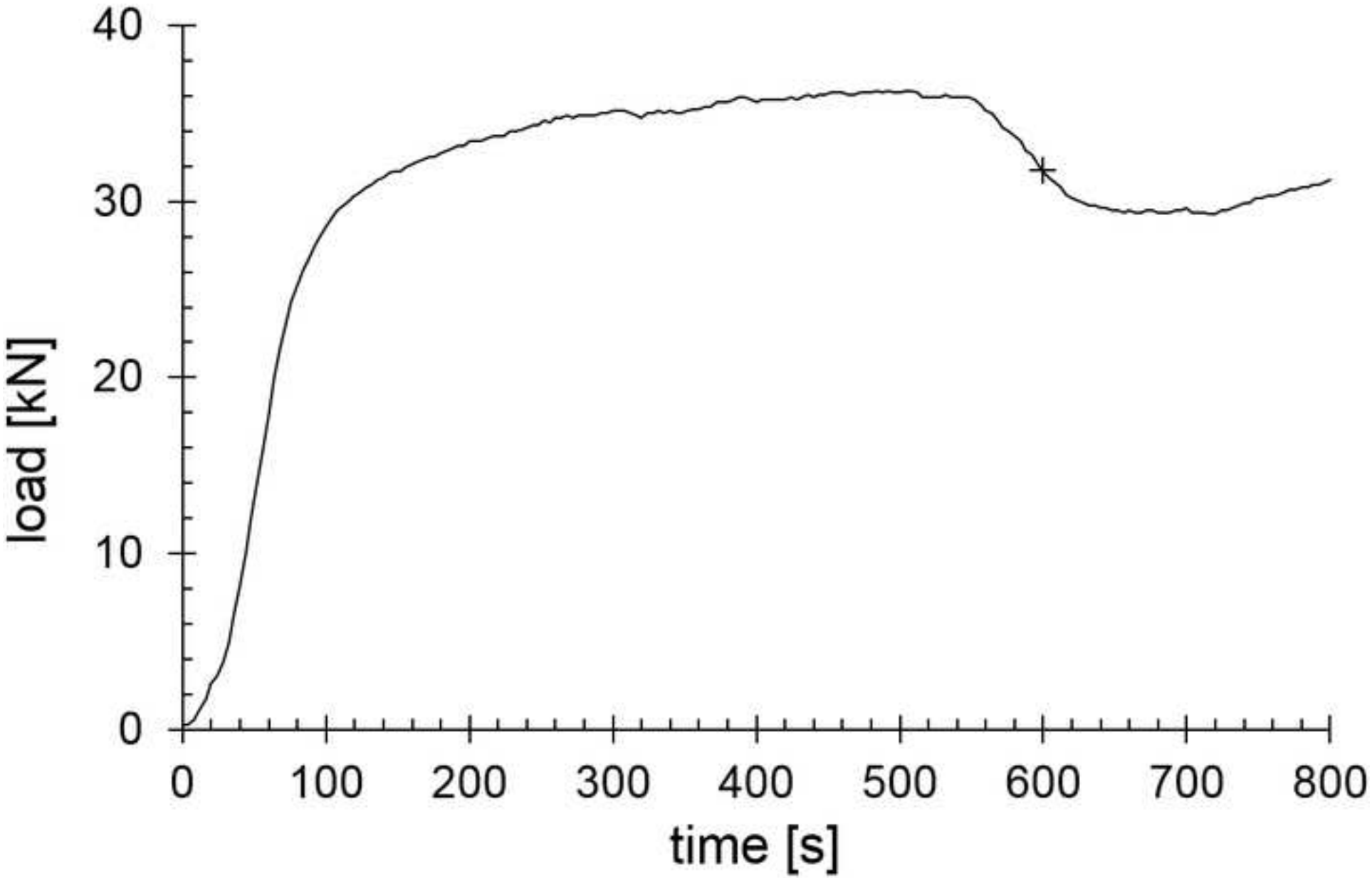

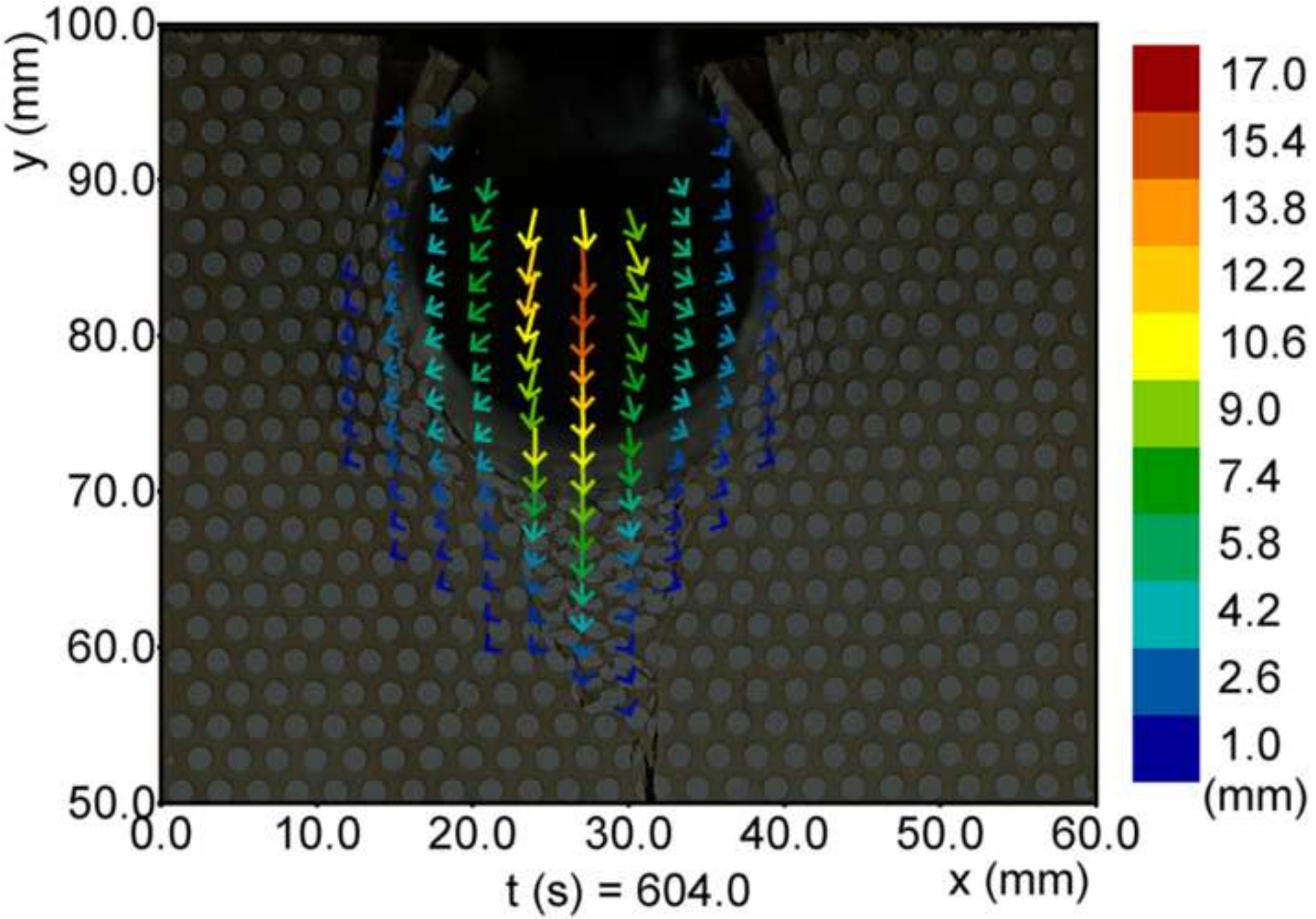

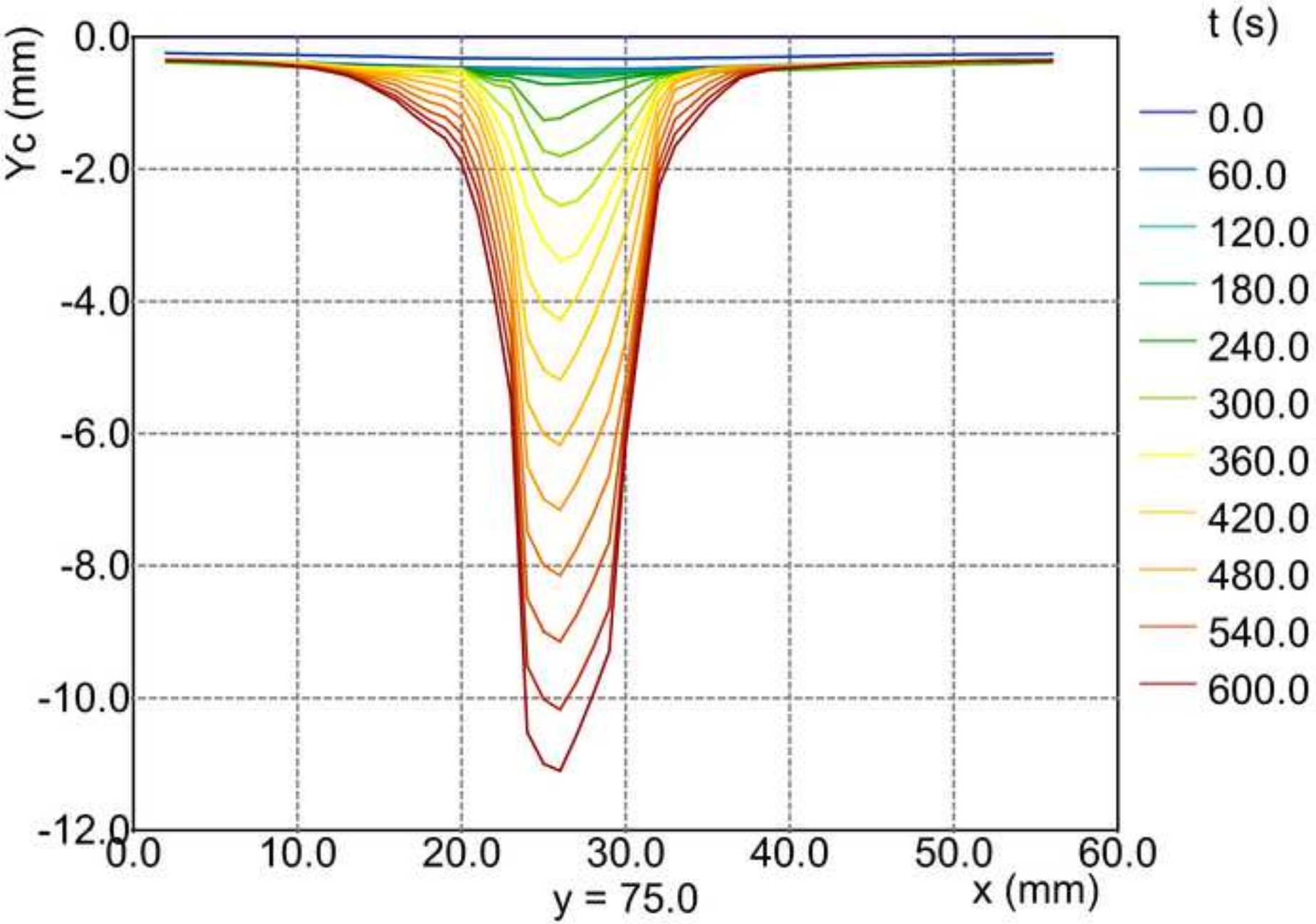

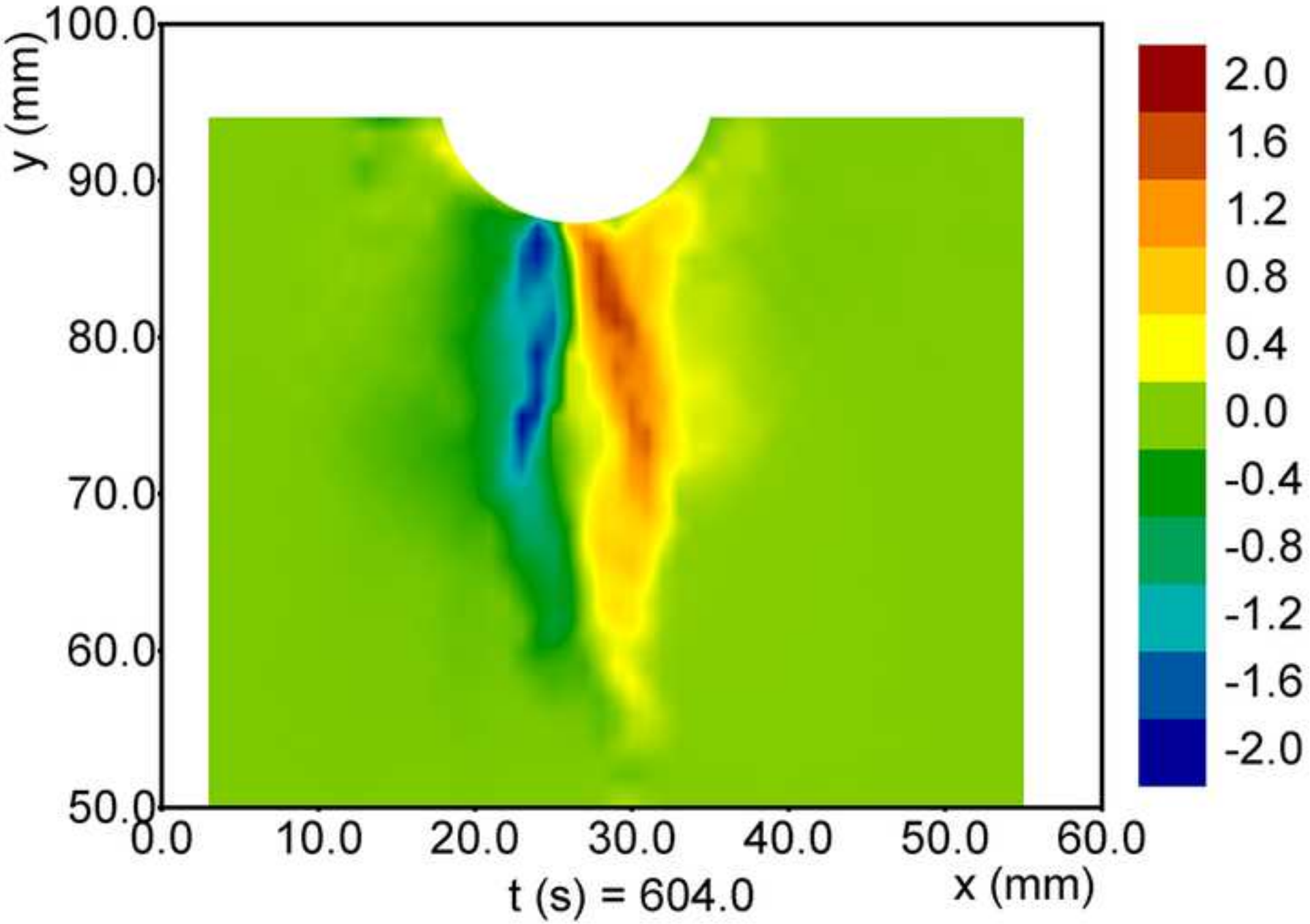

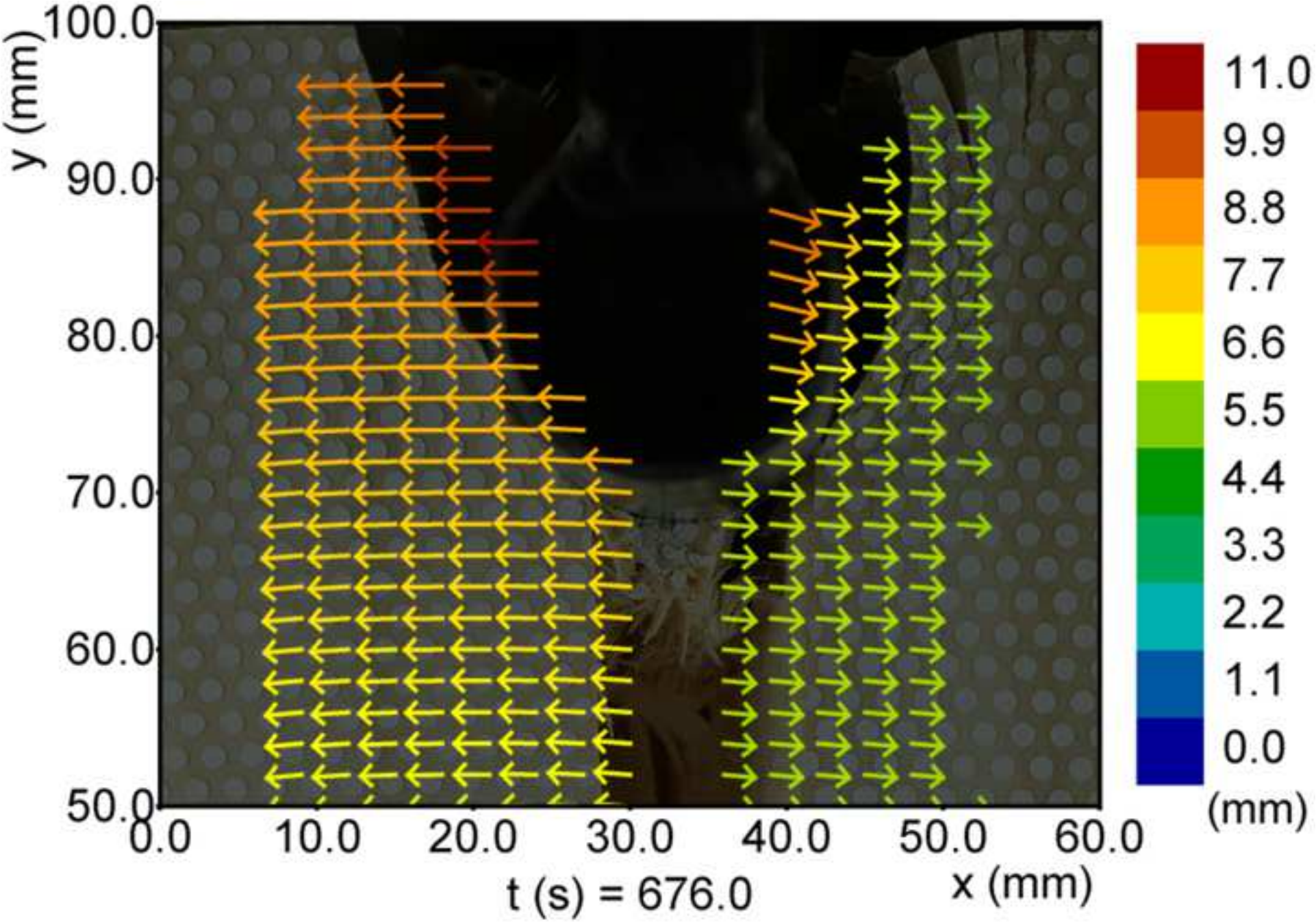

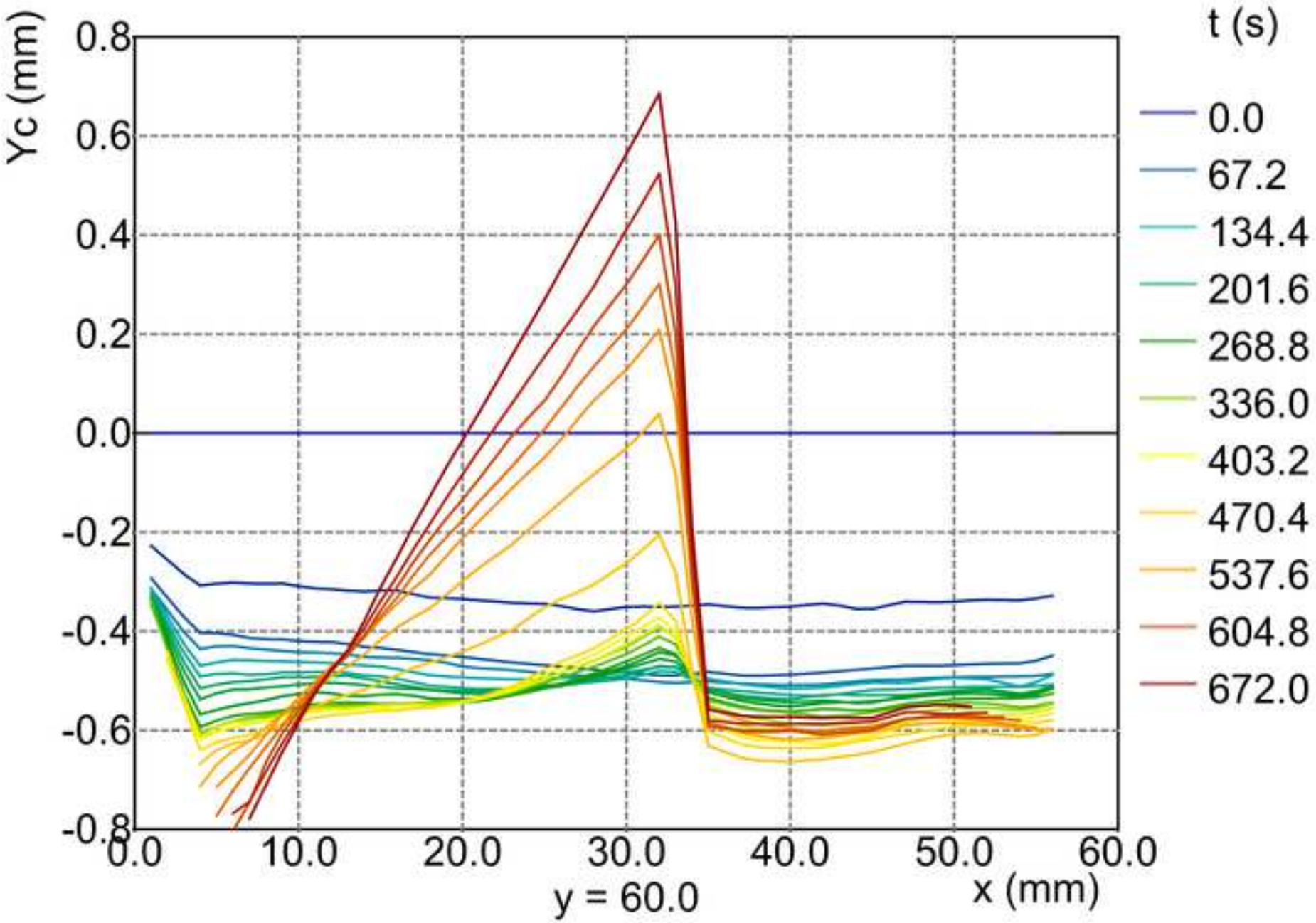

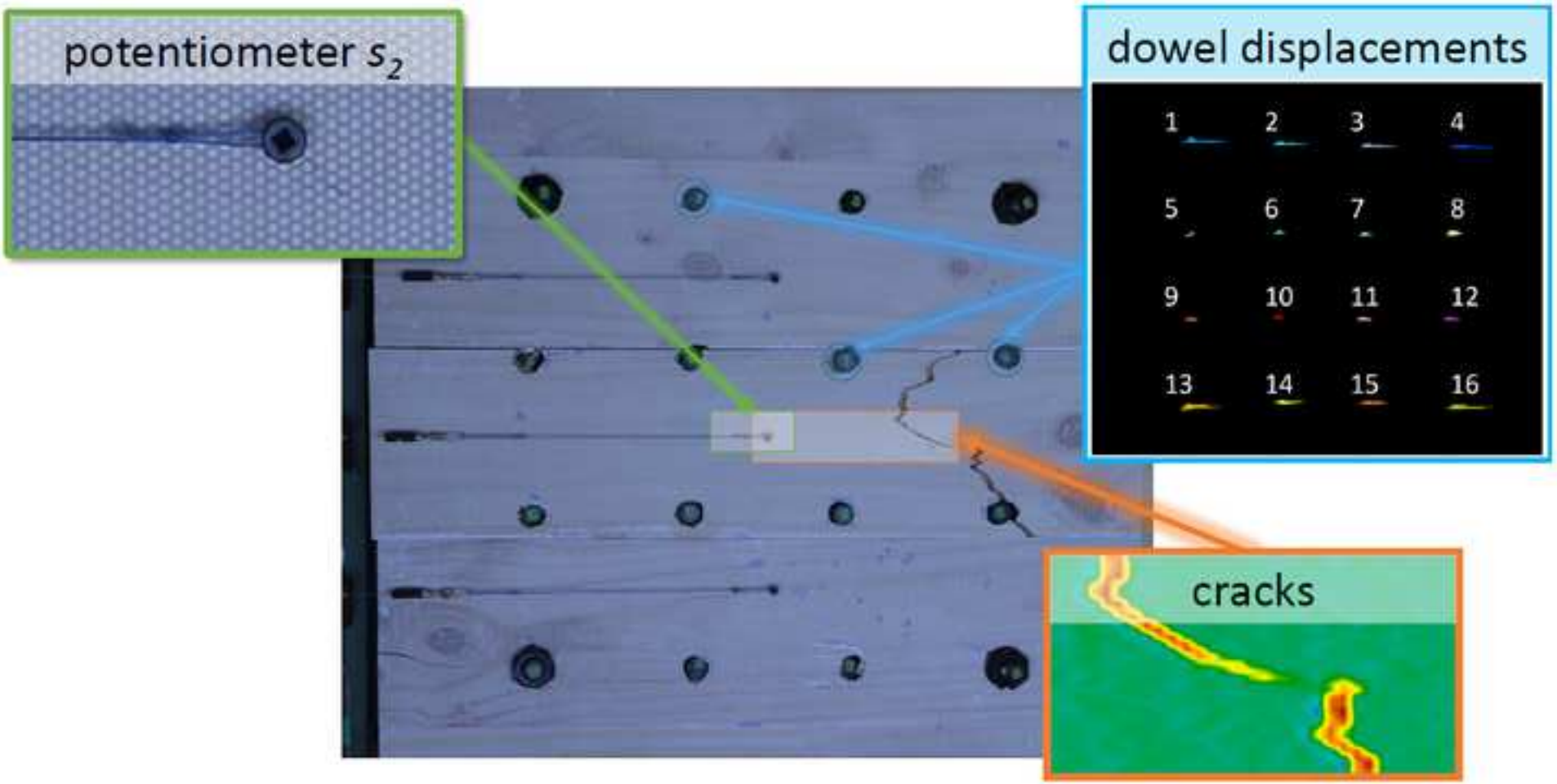

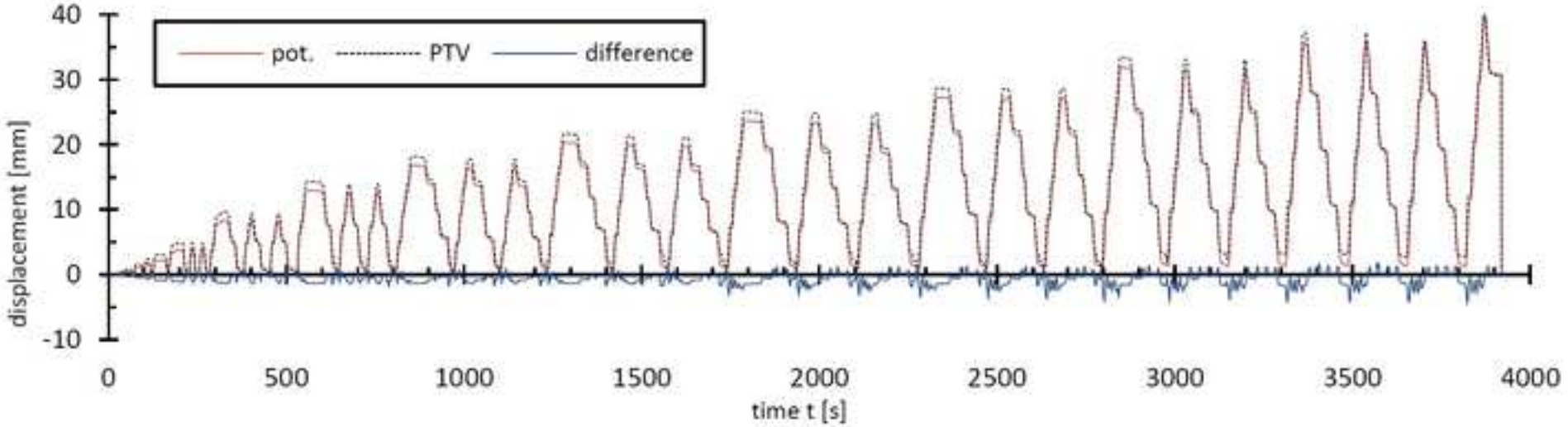

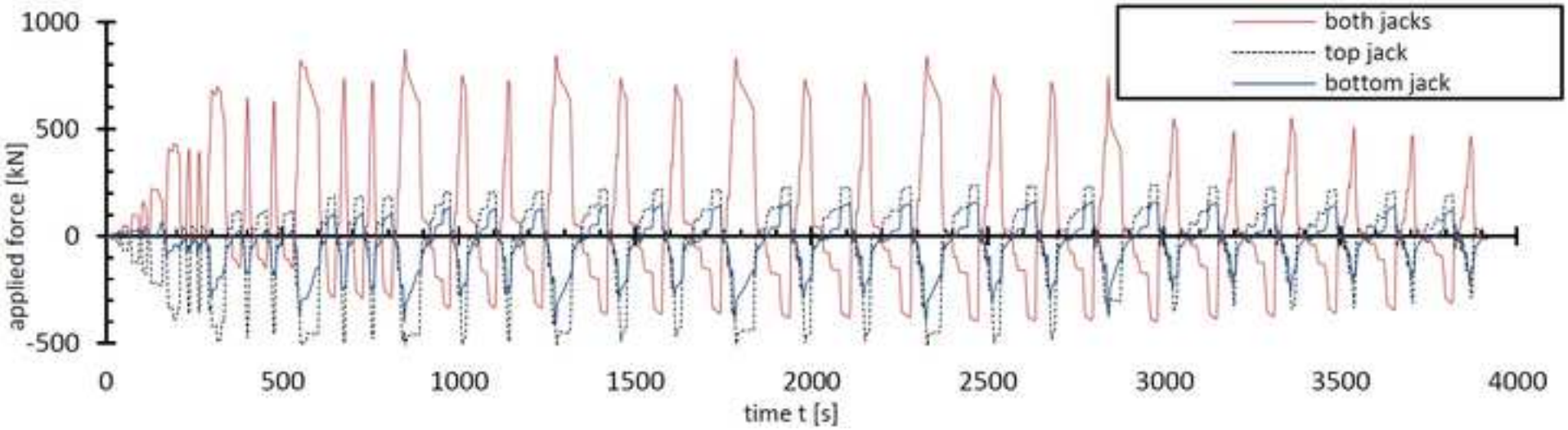

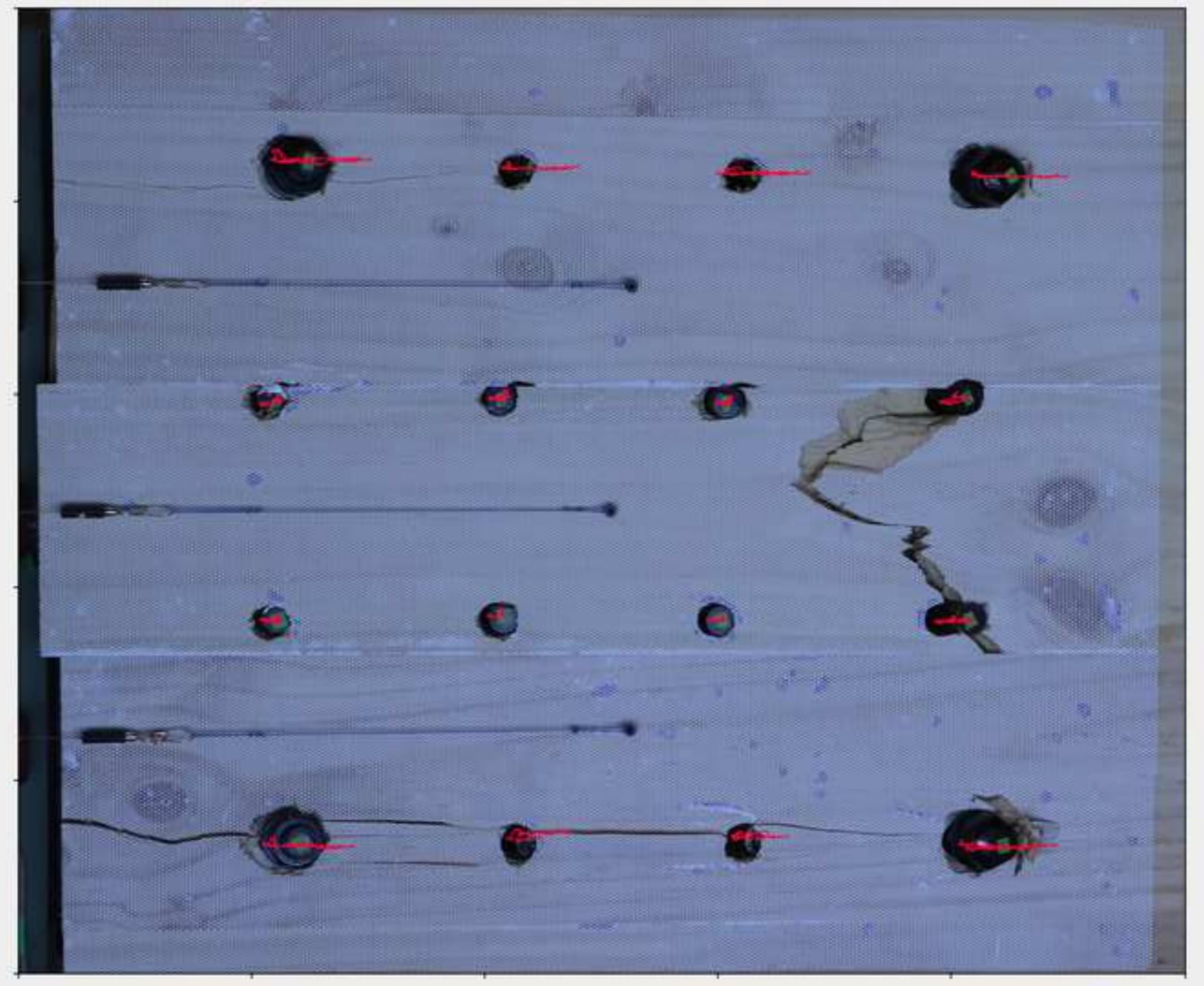

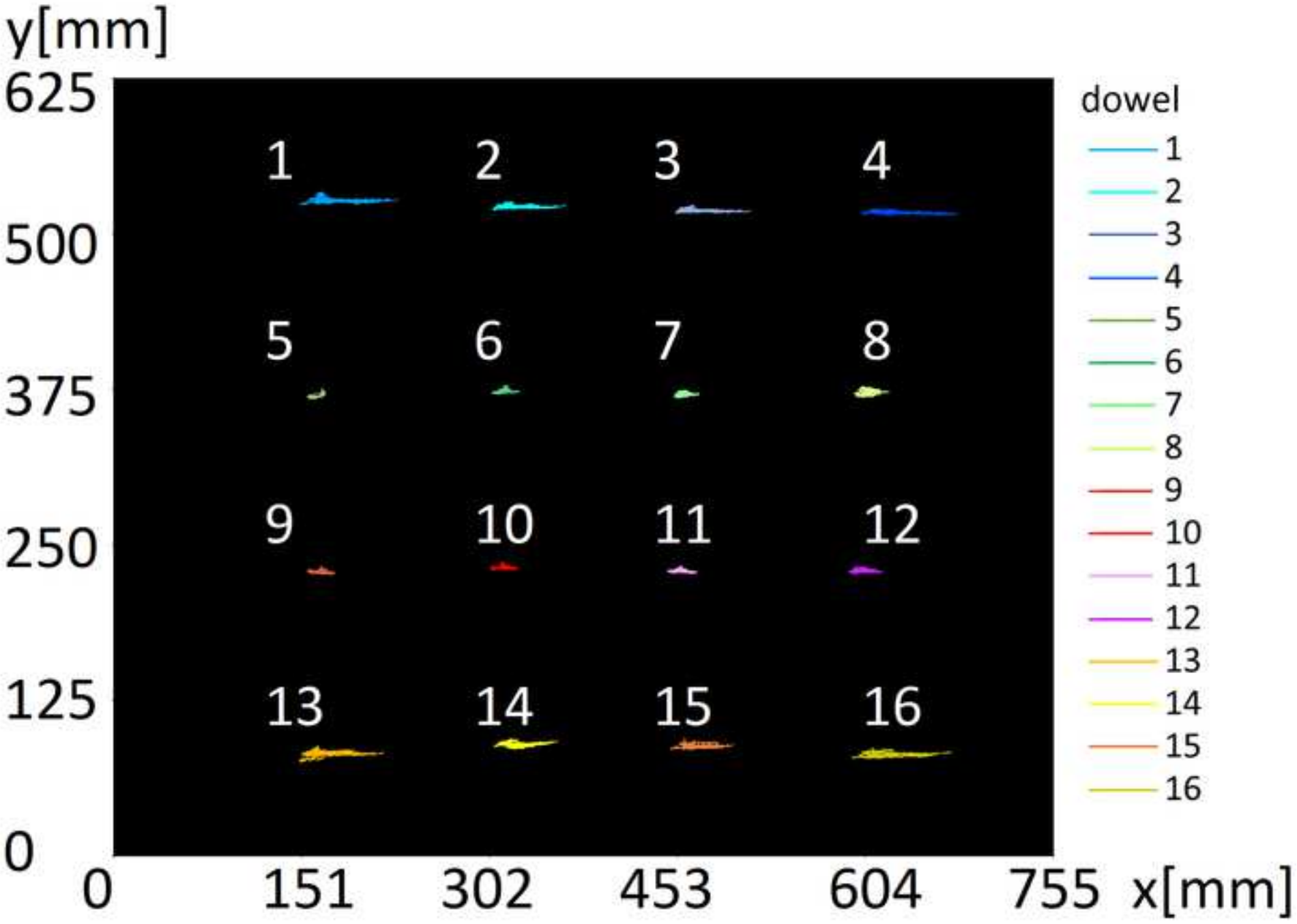

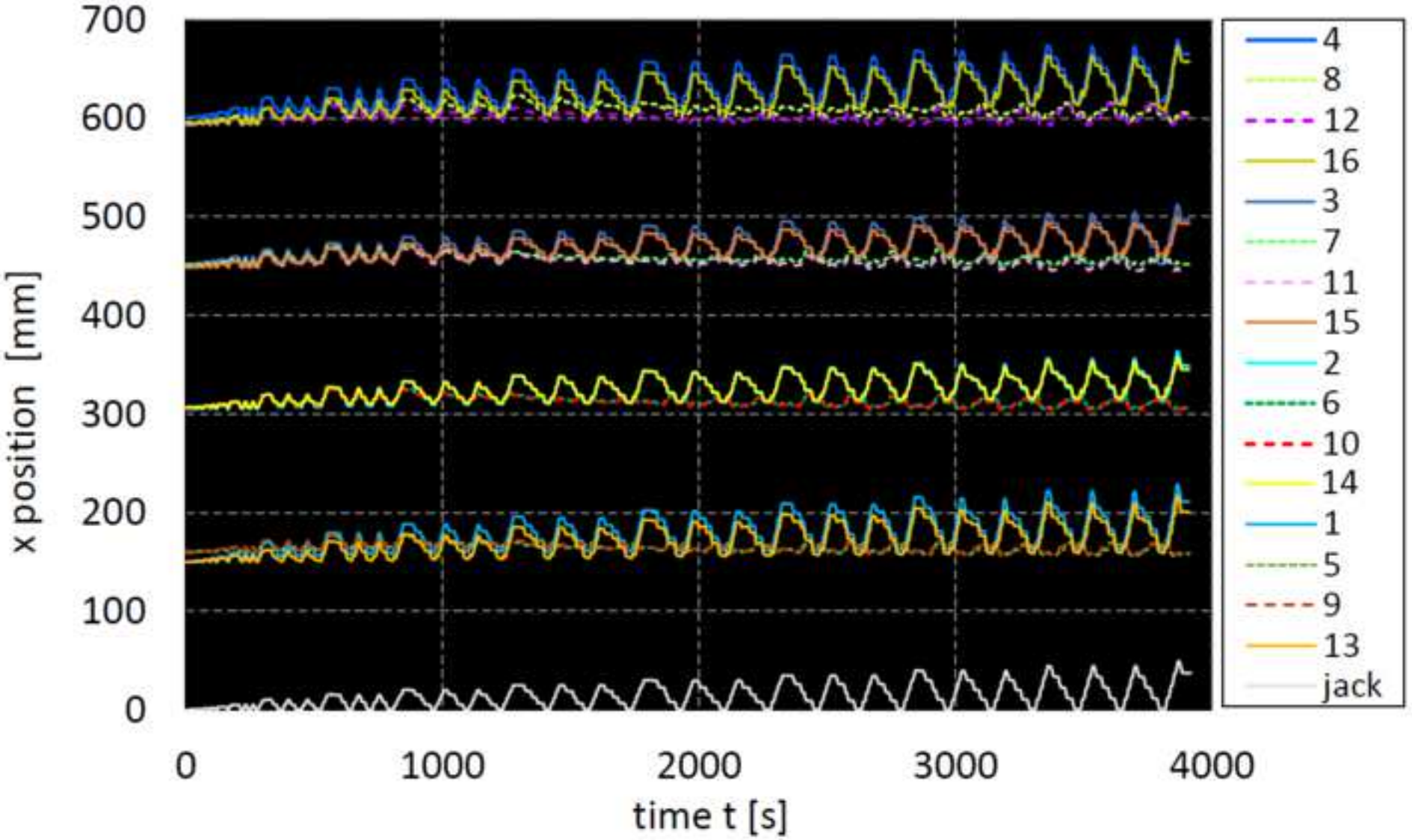

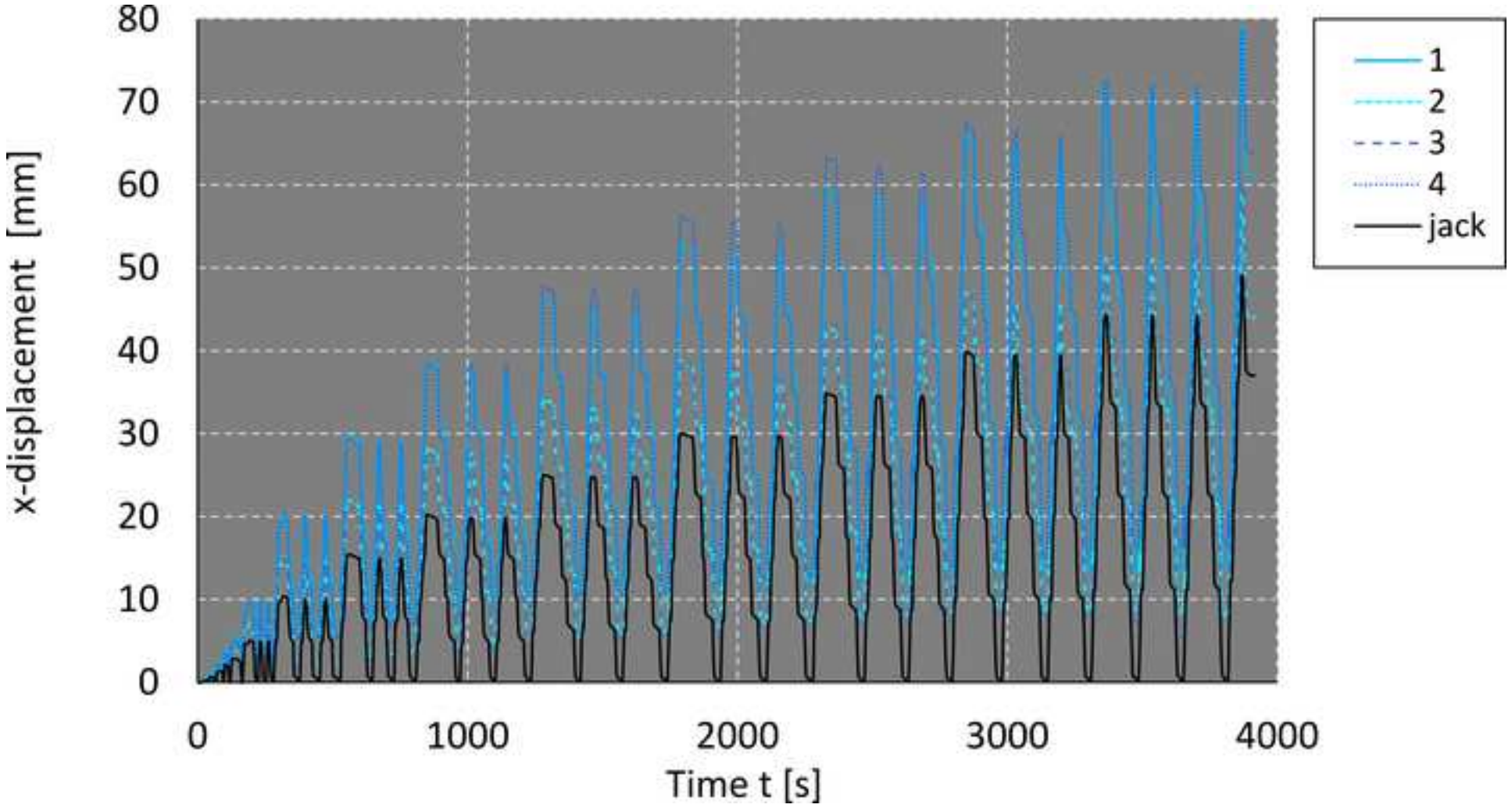

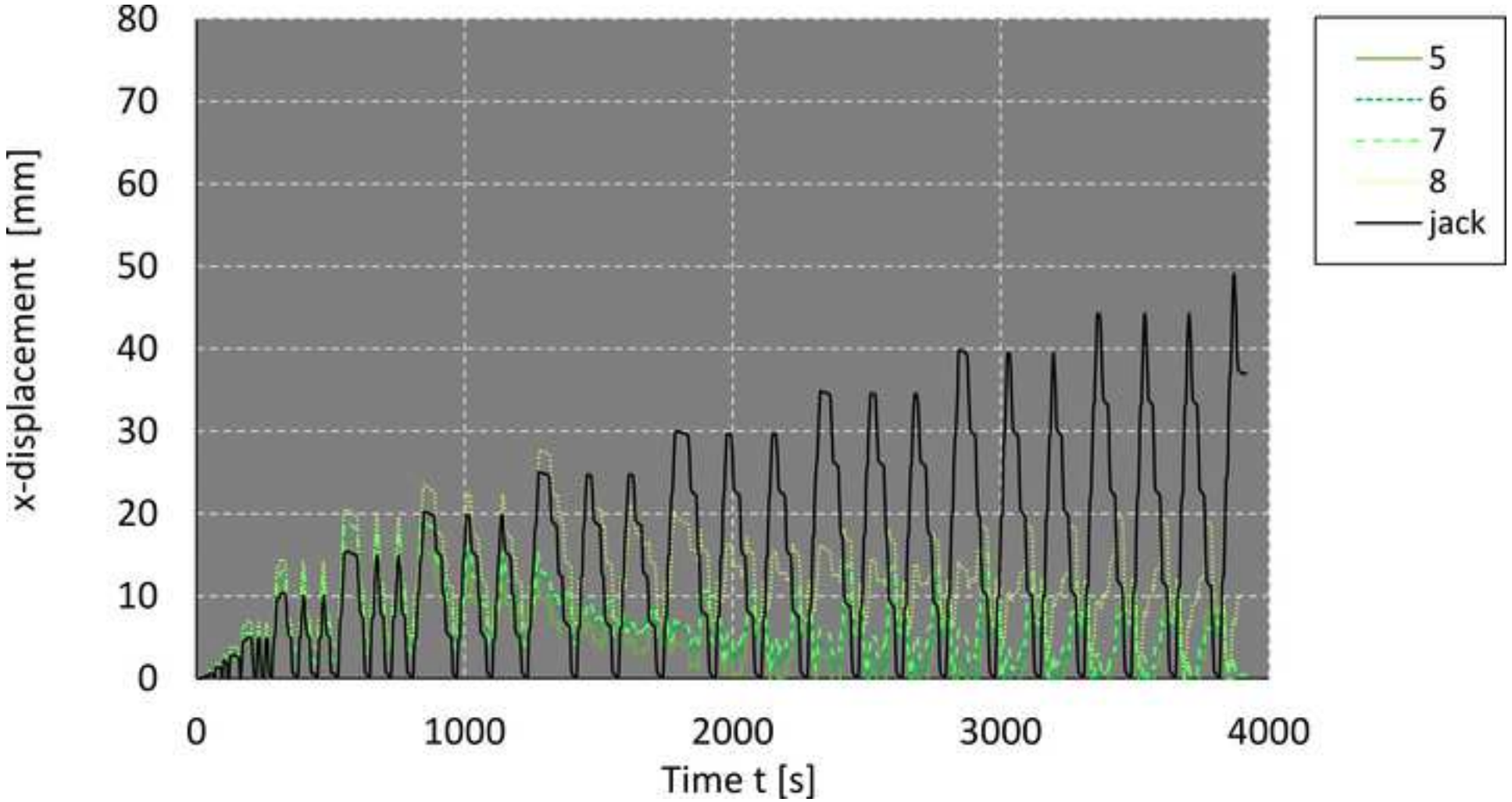

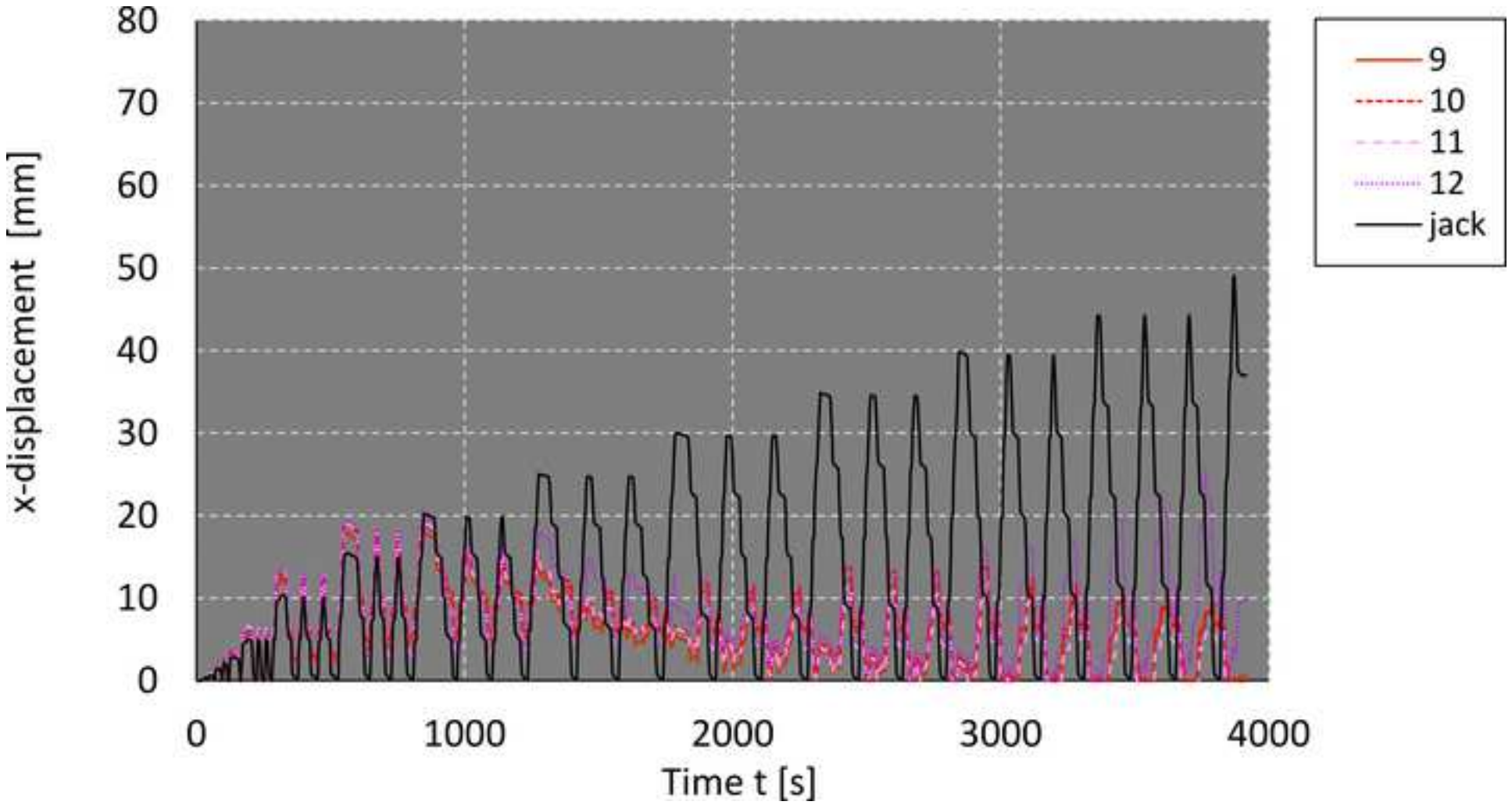

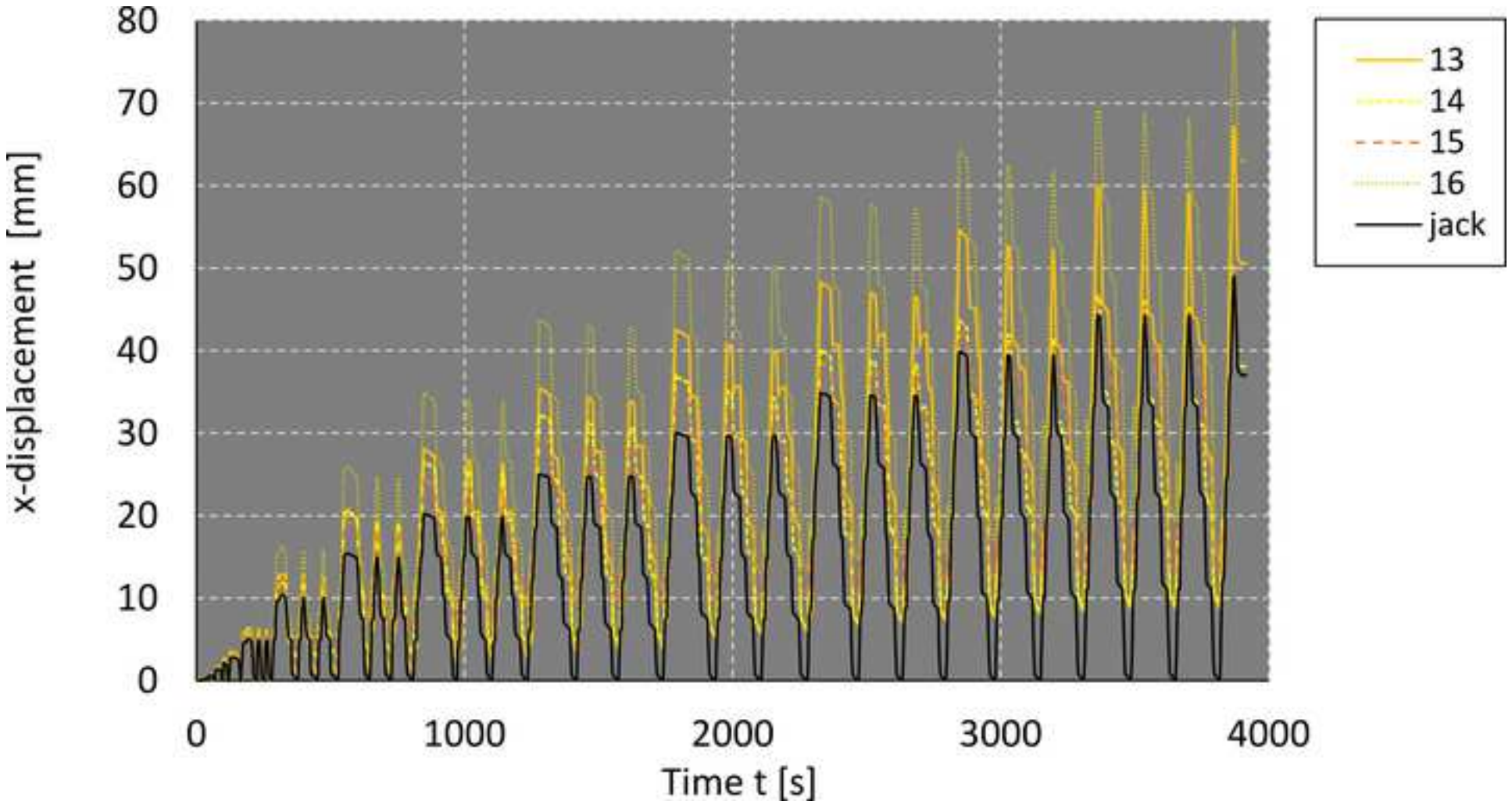

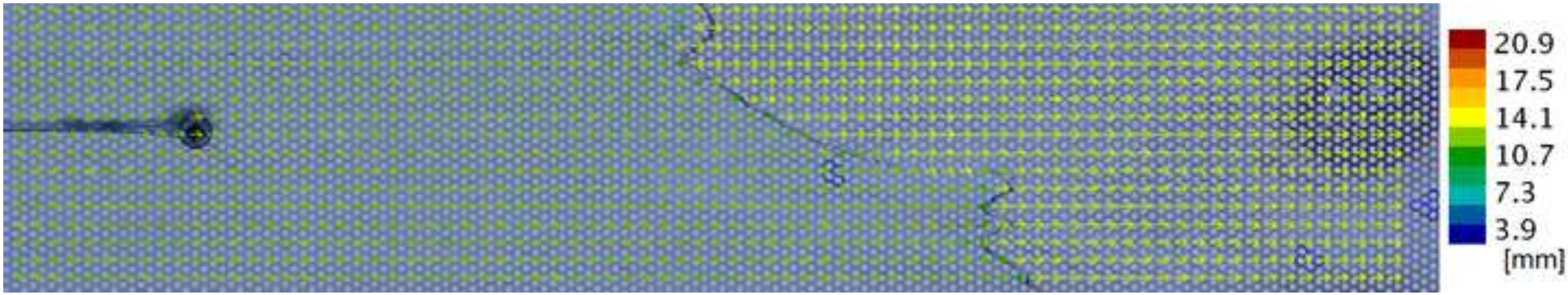

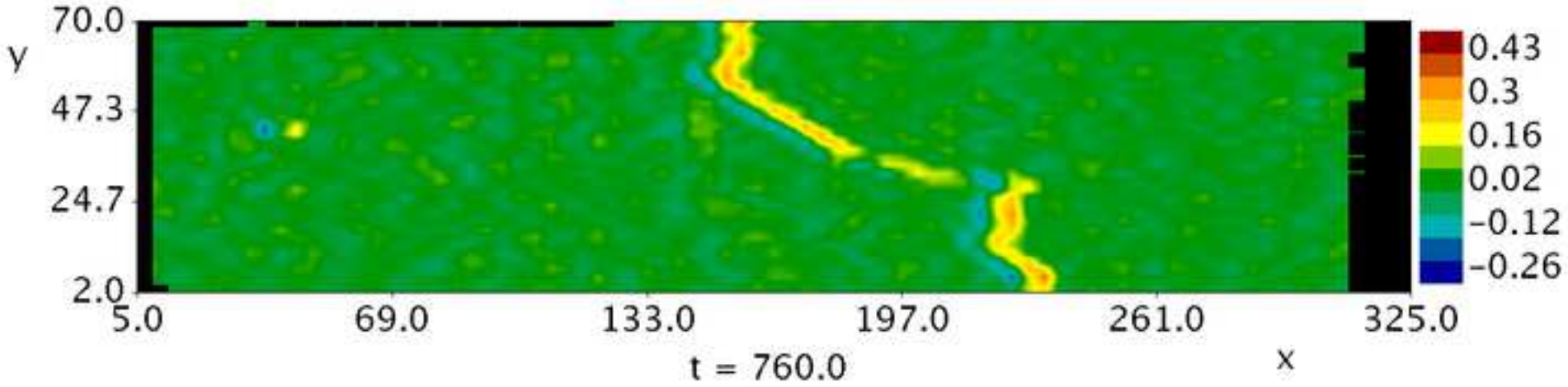

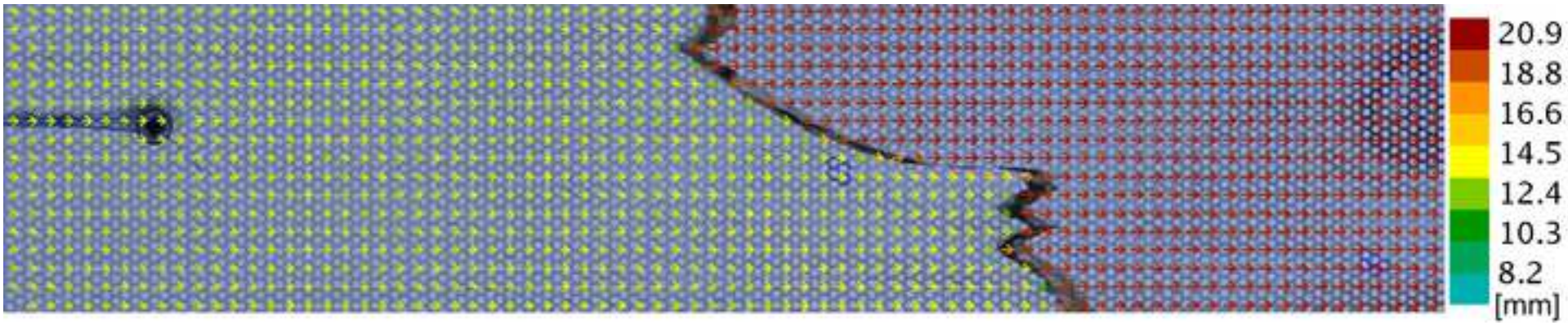

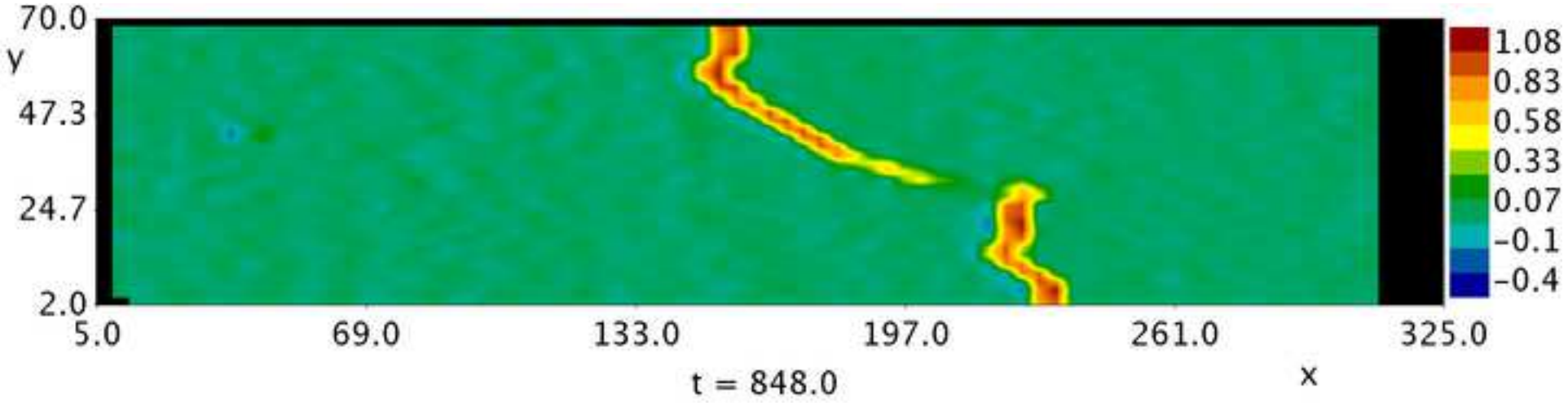

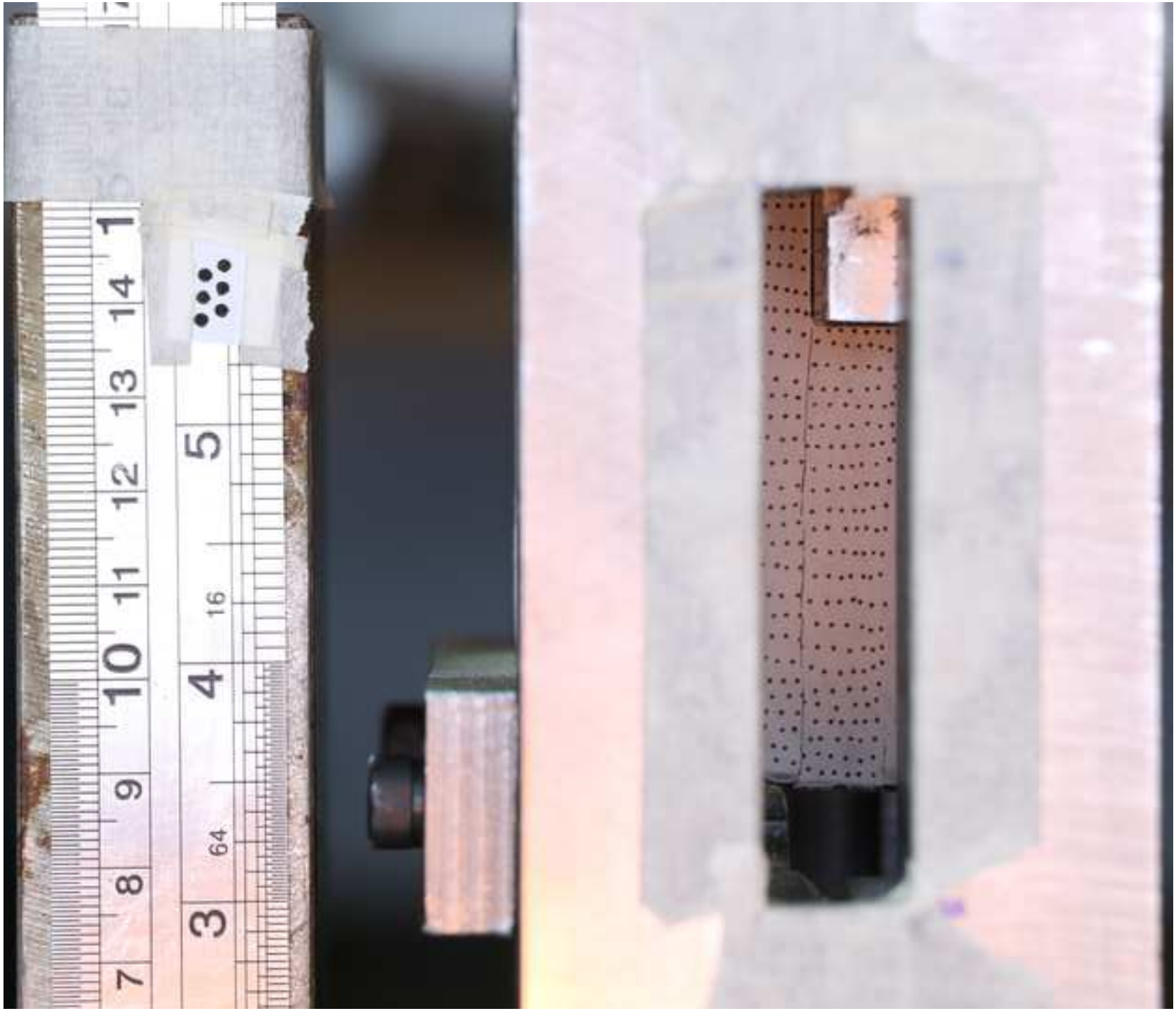

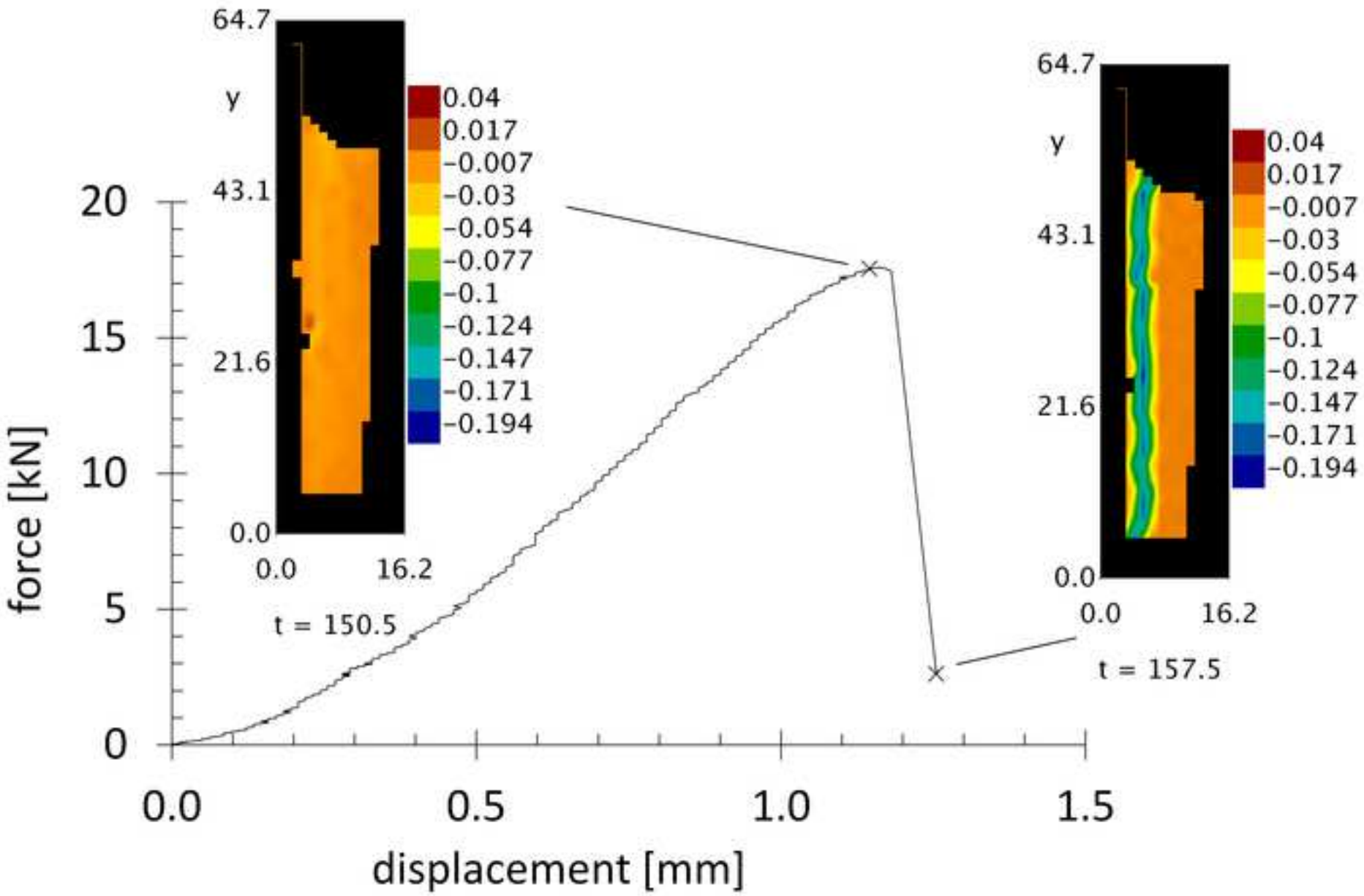

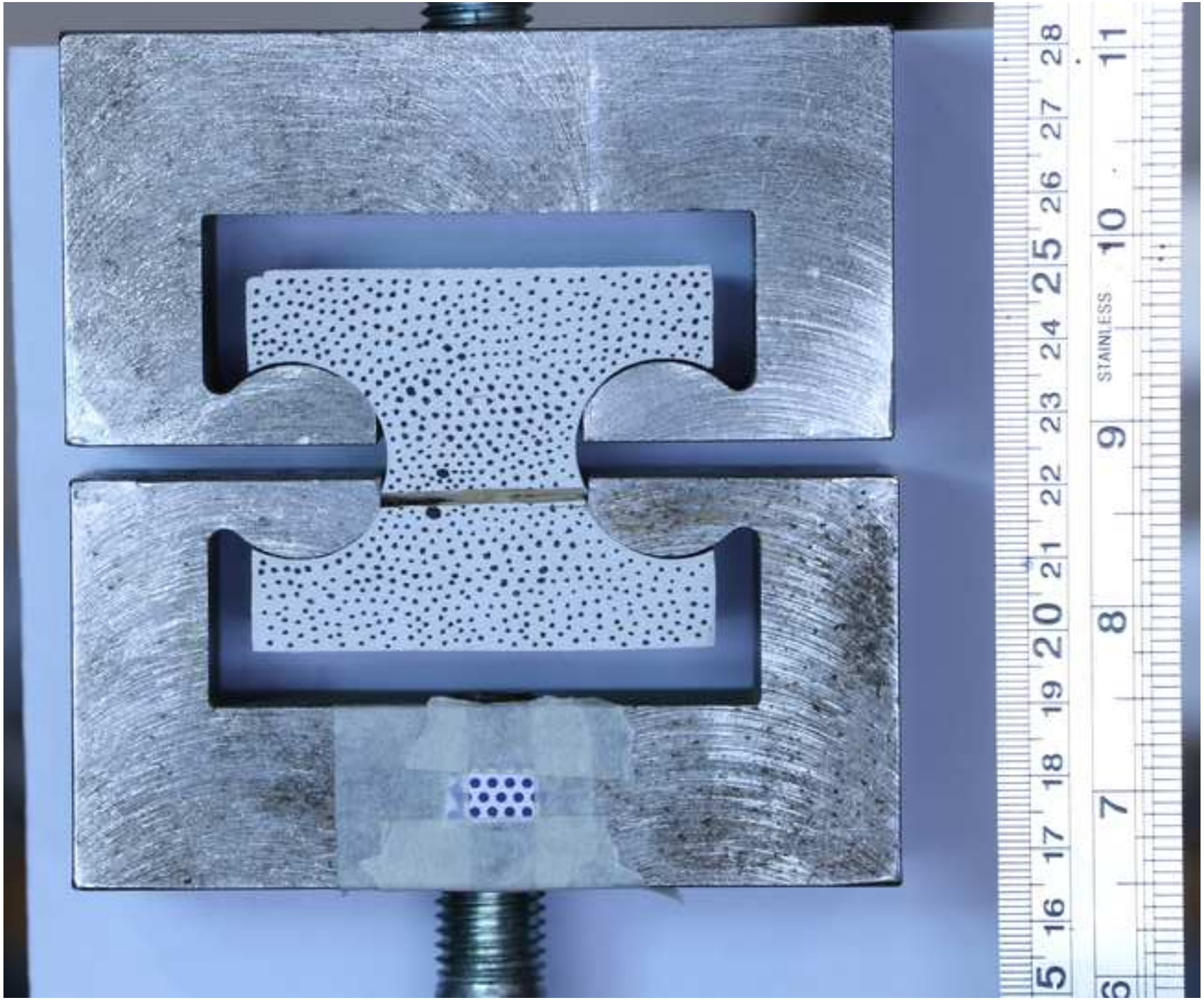

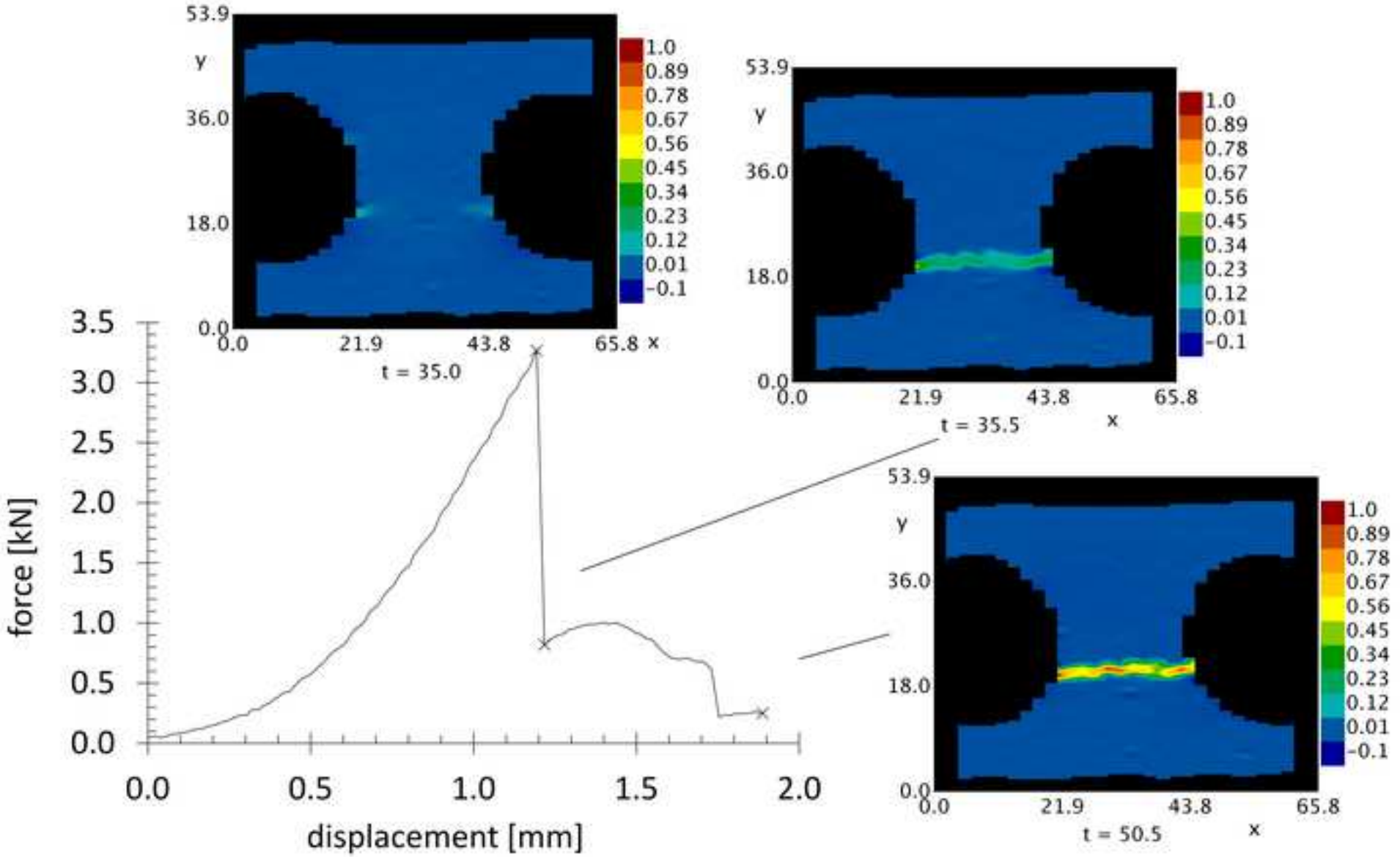

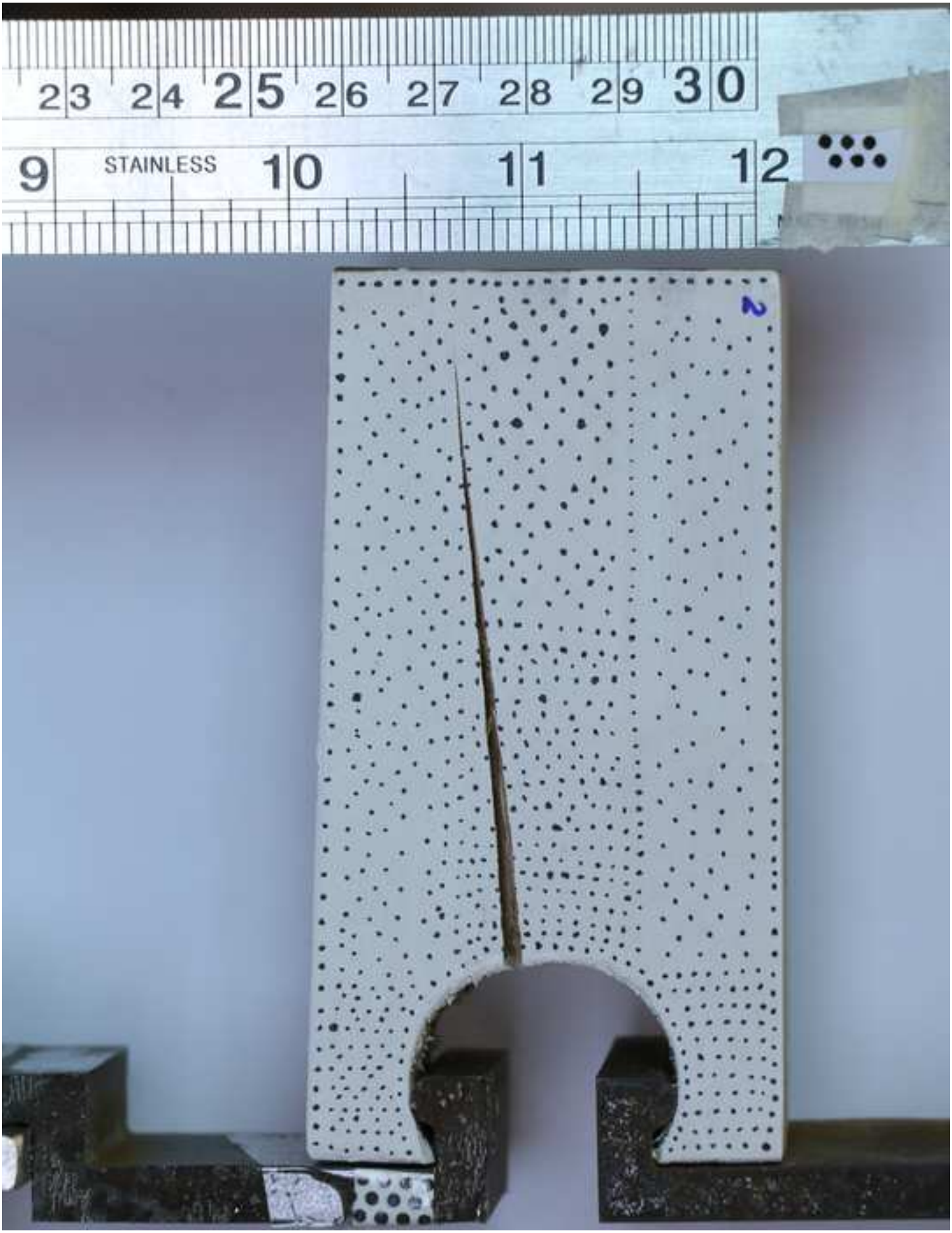

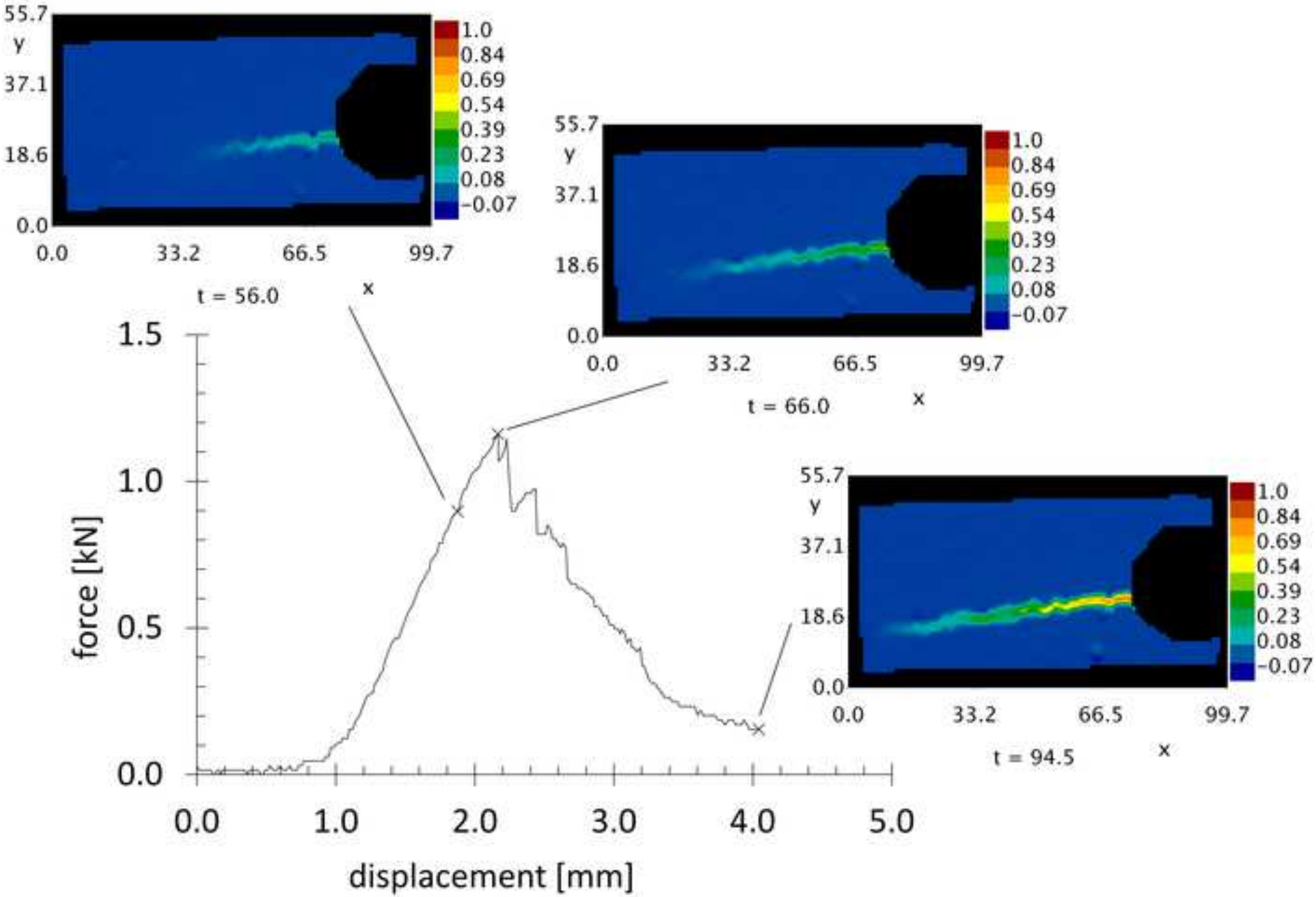

Reviewer #1:
The reviewer appreciates comments and answers that have been made by the authors of the paper. Nevertheless, the reviewer asks authors of the paper to position the experimental technique used here in relation to DIC and Grid Method, by giving advantages and disadvantages of PTV technique, based on articles that use at least one of the 3 techniques for paper applications.

Thank you for this comment. Several highlighted sentences have been added to explain the choice of PTV over DIC and MTM. Furthermore, a reference has been added that demonstrates the advantages of MTM (which is similar to PTV). The authors are not aware of a publication that compares PTV to these methods as PTV is not (yet) commonly used in structural engineering.